

1 **Repeated reactivation of clogged permeable pathways in epithermal gold deposits:**
2 **Kestanelik epithermal vein system, NW Turkey**

3
4 Nilay Gülyüz^{1,2*}, Zoe K. Shipton¹, İlkay Kuşcu³, Richard A. Lord¹, Nuretdin Kaymakçı⁴, Erhan Gülyüz² &
5 David R. Gladwell⁵

6
7 ¹*Department of Civil and Environmental Engineering, University of Strathclyde, Glasgow G1 1XQ, UK*

8 ²*Department of Geological Engineering, Yüzüncü Yıl University, 65080, Van, Turkey*

9 ³*Department of Geological Engineering, Muğla Sıtkı Koçman University, 48000, Muğla, Turkey*

10 ⁴*Department of Geological Engineering, Middle East Technical University, 06800, Ankara, Turkey*

11 ⁵*Geochemico Consulting Incorporated, 241021 Concession 3 Allenford, Ontario N0H 1A0, Canada*

12 *Corresponding author (e-mail: nilay.gulyuz@strath.ac.uk)

13
14 **Abstract:** This study presents a detailed study of the dimensions, geometry, textures and breccias of
15 a well-exposed epithermal vein system, the Kestanelik gold deposit in the Biga Peninsula, NW Turkey
16 and investigates the permeability enhancement mechanisms in epithermal gold deposits. Here
17 mineralisation is associated with quartz veins up to 13.6 m thick. Vein textures and breccia
18 components indicate repeated sealing and subsequent brecciation of wall rock and pre-existing vein
19 infill. Field and petrographic analyses characterize E-W trending veins as left lateral faults, whilst NE-
20 SW trending veins are extensional (Mode I) fractures. Cataclasite and tectonic breccia of wall rocks
21 and early quartz, hydrothermal crackle breccias, and matrix supported chaotic breccias of pre-
22 existing vein infill, all of which are cemented by late iron-oxide-bearing quartz, indicate that co-
23 seismic rupturing and hydraulic fracturing are two major permeability enhancement mechanisms. In
24 addition, transient variations in local stress direction, caused by syn-mineralisation dyke intrusion,
25 may have enhanced permeability on mis-oriented surfaces and at locations where the dip changes.
26 This study emphasizes the importance of understanding structural geology and kinematics as
27 controls on the location of boiling and mineralisation mechanisms in epithermal gold deposits.

28
29 **Key words:** epithermal, veins, permeability, kinematics, gold, earthquakes

30

31 **Abbreviated title:** Repeated reactivation of clogged permeable pathways

32

33 Epithermal deposits originate in the upper, brittle crust in regions with active magmatic and
34 geothermal activity. Mineralisation in these deposits is dominantly hosted by veins or stockworks,
35 confirming that brittle fault and fracture systems play a major role in the circulation of hydrothermal
36 fluids (Buchanan 1981; Hedenquist & Lowenstern 1994; Curewitz & Karson 1997). The ore and
37 gangue minerals in the veins are typically the result of multiphase precipitation (Spurr 1925; Hulin
38 1929; Buchanan 1981; Sibson 1987; Hedenquist *et al.* 2000), and associated with repeated and
39 episodic fluid flow rather than a steady-state process (Sibson 1987; Micklethwaite & Cox 2004;
40 Woodcock *et al.* 2007). Additionally, radiometric dating of some hydrothermal deposits indicates that
41 permeability creation and hydrothermal fluid circulation could take place over thousands to tens of
42 thousands of years (Fournier 1989; Lalou *et al.* 1993). This could be as long as millions of years in
43 major porphyry systems (Sillitoe 2010). Understanding how subsequent permeability enhancement
44 can be achieved after the deposition of minerals in fractures and faults chokes permeable pathways
45 and restricts fluid flow is crucial.

46 Several precipitation mechanisms from the circulating hydrothermal solutions are invoked for both
47 high and low sulphidation epithermal systems such as boiling, oxidation, fluid mixing, adiabatic
48 boiling, pH change etc. The most favourable precipitation mechanism in low sulphidation epithermal
49 systems is boiling. Epithermal fluids rise from depth along structural pathways at high temperatures
50 under suitable pressure to prevent boiling. When the pressure drops suddenly (e.g. through faulting
51 or fracturing-related dilation), boiling occurs. Even small magnitude earthquakes ($M_w < 2$) can trigger
52 boiling (Sanchez-Alfaro *et al.* 2016). Changes in the fluid chemistry by boiling result in precipitation of
53 base metals at deeper levels, and precious ore and gangue minerals at relatively shallower depths
54 until the open spaces are sealed, and fracture permeability is occluded or lost (Buchanan 1981;
55 Henley 1985; Hedenquist *et al.* 2000).

56 The mineralogical and geochemical aspects of low sulphidation (LS) epithermal systems are well
57 known (e.g. Buchanan 1981; White & Hedenquist 1990; Hedenquist & Lowenstern 1994; White &
58 Hedenquist 1995; Hedenquist *et al.* 2000; Sillitoe & Hedenquist 2003; Simmons *et al.* 2005).
59 However, limited studies exist on the fluid flow and permeability enhancement mechanisms in LS
60 epithermal veins. The existing studies generally focus on the role and significance of geometric and
61 mechanical aspects of the fault-fracture systems on the epithermal deposits. Terminations of

62 individual faults and locations of multiple fault interaction are areas of high fracture density and
63 connectivity and are therefore likely to localize high fluid flow (Curewitz & Karson 1997; Cox *et al.*
64 2001; Cox 2005). Observation from fossil epithermal deposits shows that epithermal mineralisation is
65 often located in dilational jogs within fault systems (Sibson 1987). Major faults can be either
66 important barriers or conduits to fluid flow (Caine *et al.* 1996; Rowland & Sibson 2004), while the
67 permeability may be nonuniform along the fault depending on the relationship between the variable
68 strike of the fault and the orientation of the local stress direction (Micklethwaite *et al.* 2010).
69 Permeability can also be developed or maintained along individual fault segments because
70 interconnected fractures and subsidiary faults form in the wall rocks where damage zone occurs
71 adjacent to a fault core (Caine *et al.* 1996; Davatzes *et al.* 2005). The damage zone structures that are
72 permeable may also change position over geological time (Woodcock *et al.* 2007; Burnside *et al.*
73 2013). Micklethwaite & Cox (2004, 2006) argued that if the event responsible for opening permeable
74 pathways is an earthquake, although the permeability of the fault where the mainshock occurs may
75 rapidly be lost due to the precipitation of hydrothermal minerals, enhanced fluid flow may occur
76 along the structures where aftershock ruptures focus and the location of these structures are
77 predictable based on stress transfer modelling.

78 Rather than focusing on structural controls at the fault system-scale, this study presents the
79 dimensions, geometry, kinematics, textures and breccias of the individual veins. We examine the
80 very shallowest levels of a well-exposed epithermal vein system at the Kestanelik gold deposit (Biga
81 Peninsula, NW Turkey). Field and drill core data are used to understand the deformation mechanisms
82 and kinematics of the vein system, specifically focussing on determining the origin of the fracture
83 zones (a shear fracture or extensional fracture zone) along which the mineralisation has occurred.
84 Implications for the vein-scale permeability enhancement mechanisms and effective prospect
85 evaluation in epithermal gold deposits are explored.

86 This study has revealed significant new microstructural evidence for reactivation along the vein-wall
87 rock contact and associated permeability development and fluid flow after the veins were clogged.
88 These findings support the few earlier studies of the permeability enhancement mechanisms and
89 fluid flow in epithermal systems (e.g. Sibson 1987; Cox *et al.* 2001; Micklethwaite & Cox 2004;
90 Micklethwaite 2009) but are also the first detailed textural studies of the permeability enhancement
91 mechanisms. It also emphasizes the importance of understanding structural controls and triggers for
92 mineralisation that are evident from structures and textures during the exploration of epithermal
93 gold deposits.

95 **Kestanelik epithermal gold deposit**

96 The Kestanelik gold deposit is located in the Biga Peninsula, NW Turkey approximately 45 km
97 northeast of Çanakkale. Paleozoic metamorphic and ophiolitic basement rocks are cut by various
98 Eocene to Miocene plutons and covered by Cenozoic volcanic and sedimentary rock units (Okay *et al.*
99 1996) (Fig. 1). Starting from the Middle Eocene, extensive magmatism prevailed in NW Turkey that
100 changed in character from calc-alkaline to alkaline in the Middle Miocene (e.g. Altunkaynak & Genç
101 2008).

102 The gold mineralisation in the Kestanelik deposit is associated with quartz veins that crop out over an
103 area of nearly 2 km² (Fig. 2). The veins are hosted by Paleozoic mica schist (Okay *et al.* 1990) and
104 quartz-feldspar-hornblende (QFH) porphyry that yielded an age of 43.34±0.85 Ma (K-feldspar Ar-Ar
105 age) at the Madendağ low sulphidation deposit (Ünal-İmer *et al.* 2013) ~45 km to the southwest of
106 the Kestanelik deposit. The oldest sedimentary rock unconformably covering the mineralized veins is
107 Priabonian limy sandstone, and the youngest host rock for the veins is the QFH porphyry. We
108 therefore presume that the age of the mineralisation is Late Lutetian-Early Priabonian (Middle to
109 Late Eocene), suggesting that the Kestanelik gold deposit has a genetic link with the Eocene calc-
110 alkaline magmatism in the region.

111 The Kestanelik epithermal gold deposit is a LS epithermal type. Classification as a LS epithermal
112 system is based on the vein-ore textures, and predominant ore and gangue mineralogy. Although we
113 have not identified adularia, a common mineral in low sulphidation systems, pseudo-bladed quartz
114 replacing bladed carbonate mineral is typical in LS systems. We also observed colloform to crustiform
115 quartz, comb to cockade ore-vein textures, and hydrothermal breccias. Ore minerals are native gold
116 and accessory silver. Quartz veins generally have moderate to high gold grades (Au range in 1-20 g/t)
117 and the Au:Ag ratio is generally in the range of 2:1 to 1:1. Gangue minerals are principally quartz,
118 amethyst and chalcedony with pyrite and accessory chalcopryrite, sphalerite and galena
119 dissemination in the vein quartz.

120 Vein quartz textures observed in the field are types typically ascribed to open space filling (such as
121 cockade and comb textures) and replacement (such as saccharoidal and pseudo-bladed textures).
122 The most striking feature of the veins is brecciation. Quartz vein breccias are generally composed of
123 monomictic to polymictic clasts of host rocks and/or earlier phase(s) cemented by quartz-iron-oxide.
124 Clasts of earlier breccia within some breccias indicate that at least two phases of brecciation
125 occurred in the area. The absence of silica sinter, a diagnostic paleosurface indicator in LS epithermal
126 systems, suggests that the uppermost parts of the epithermal system have been eroded.

127 The QFH porphyry in the field area is always altered with some typical argillic alteration minerals
128 (illite and smectite). These assemblages were also observed in initial PIMA analyses (Hedenquist
129 2011). Alteration is more intense around field exposure and drill core samples of the veins,
130 suggesting that the veins were the source of the alteration fluids. In deeper drill cores the degree of
131 alteration is lower. All of the observed porphyry outcrops are altered, the furthest is up to 500m
132 away from the nearest observed vein. This is very wide for a vein-associated alteration halo (more
133 typically a few tens of meters, Hedenquist *et al.* 2000).

134 A mafic dyke that cuts and contains fragments of altered QFH porphyry (xenoliths) is observed in a
135 drill core. Adjacent to the dyke, a polymictic breccia contains clasts of the same dyke and vein quartz
136 in turn cemented by quartz. This textural evidence indicates that the vein-related alteration was
137 already present when the dyke was intruded, suggesting contemporaneous mineralisation and dyke
138 intrusion (Fig. 3). This dyke is therefore likely to be related to Cenozoic magmatism in the Biga
139 Peninsula (e.g. Altunkaynak & Genç 2008).

140 The field area is cut by the deeply incised Kestanelik River, providing a topographic exposure interval
141 of ~150 m. The post-mineralisation limy sandstone records to the SW to a mean dip of 29° and
142 direction of 110°. This tilting is exceeded by the effect of the river incision meaning that the NE flank
143 of the valley is equivalent to a pseudo cross-section through the very shallowest part of the
144 hydrothermal system with the paleo-depth of vein emplacement increasing slightly to the SW of the
145 field area.

146

147 **Characteristics of the epithermal vein system**

148

149 The gold mineralisation in the area is hosted by major quartz veins, wall rock veins and sheeted veins
150 in the river valley. Outcrop geometries of the veins were mapped using a Trimble GPS (± 0.1 cm).
151 Vein-related detailed structural data (attitude, thickness, infill type, length, and typology) were
152 collected from surface exposures and outcrops along the creeks. The structural data were plotted
153 using the software package Stereonet (Allmendinger *et al.* 2013; Cardonzo & Allmendinger 2013) and
154 used to calculate the paleostress field at the time of gold mineralisation. In addition, observations
155 were made of the host rock deformation around the veins both in the field and in diamond cut drill
156 cores. Vein textures and breccias were examined both on exposed vein outcrops and in drill cores,
157 with the help of petrographic analysis.

158 The 3D subsurface geometries of the vein-host rock boundaries were constructed by using mapped
159 outcrop geometries, detailed field data, well-logs and geochemistry data from 396 drill holes (255
160 diamond cut and 141 reverse circulation holes) supplied by Chesser Resources, who, at the time of
161 fieldwork, were the license holder company of the Kestanelik deposit. Modelling of the top and
162 bottom surface of each vein was performed in MOVE Structural Modelling and Analysis Software
163 granted by Midland Valley's Academic Software Initiative. In addition, vertical cross sections
164 perpendicular to the vein strike were created for each vein in the MOVE Software. All veins were
165 modelled except two (the K2 and Topyurt veins) which had insufficient drillhole data.

166

167 **Major quartz veins**

168

169 There are 9 major mineralized quartz veins that form a northwest trending corridor in the deposit
170 area. These veins, from north to south include Karatepe, KK4, KK3, KK2, KK1, K1, K2, K3 and Topyurt
171 veins (Fig. 2). The host rock, strike length, mean strike, mean dip angle, and minimum and maximum
172 width of each vein from outcrop measurements are summarized in Table 1. There are two
173 mineralized vein sets in the area based on strike orientation; the first set strikes NE-SW (KK1, KK2,
174 KK3, KK4, K1, western end of K3, Topyurt) while the second one trends E-W (Karatepe, K2, eastern
175 end of K3). All of the veins are continuous (not segmented) except the segmented K3 vein and
176 Topyurt veins, however some veins have discontinuous outcrop traces due to the erosion. The NE-
177 SW sets host the majority of gold mineralisation according to the average gold grade calculations of
178 the modelled veins using the geochemical gold assay data of related drill cores (Table 2). We describe
179 these veins in turn from north to south, representing veins emplaced at increasing paleo-depths.

180 The Karatepe vein is located in the northern part of the area and hosted entirely within the QFH
181 porphyry. It is E-W oriented and extends for a strike length of 350 m. The vein dips to the south (Fig.
182 2) with an average dip of 69.8 degrees (from surface data, subsurface dips are given in Table 2). Vein
183 orientation data collected from outcrop revealed that the vein has a very corrugated strike on a
184 meter scale. The deepest drill intersection is around 160 m below surface.

185 The KK3 and KK4 veins are hosted by mica schist and strike almost NE-SW (Fig. 2). KK3 vein has a 52
186 m strike length and varies between 2 m and 8.7 m wide. The vein dips to the SE with an average dip
187 of 70.2 degrees. The KK4 vein has a strike length of 47 m and dips to the SE with an average dip of
188 68.3 degrees. The deepest drill intersection of the KK3 and KK4 veins are around 120 m and 100 m
189 below surface respectively.

190 The KK1 vein and KK2 vein are hosted by mica schist and trend approximately NE-SW (Fig. 2). The KK1
191 vein extends 150 m along strike and dips to the SE with an average dip of 76.7 degrees. Vein outcrop
192 width varies between 1.2 m and 9 m. The KK2 vein outcrop extends for 185 m, with an average dip of
193 75.8 degrees to the SE. The deepest drill intersection of the KK1 and KK2 veins are around 125 m and
194 100 m below surface respectively.

195 The NE-SW trending K1 vein extends over a strike length of around 240 m and dips to the SE (Fig. 2)
196 with an average dip of 75.1. The deepest drill intersection is around 90 m below surface.

197 The K2 vein, hosted by mica schist, has an E-W trending strike length of 86 m and dips gently to the
198 north (Fig. 2) with an average dip of 43.5 degrees.

199 The K3 vein is composed of two segments and its strike extends over 510 m (Fig. 2). The western
200 segment of the vein system (K3W vein) is hosted by mica schist and trends NE-SW with a strike
201 length of 230 m (Fig. 2). It dips to the NW with an average angle of 62.3 degrees. The deepest drill
202 intersection is around 215 m below surface. The eastern segment of the vein system (K3E vein), is
203 hosted by the QFH porphyry, extends intermittently over an E-W oriented corrugated strike with a
204 length of 280 m and dips to the north (Fig. 2) with an average angle of 71 degrees. The deepest drill
205 intersection is around 140 m below surface. The western segment of the K3 vein is more persistent
206 and thicker than its eastern part.

207 The Topyurt vein, hosted by QFH porphyry, is located in the southern part of the study area
208 perpendicular to the valley and cuts the Kestanelik River. It has 3 sub-parallel NE-SW trending
209 segments in an N-S trending zone (Fig. 2) with a total exposed strike length of 154 m and dips to NW
210 with an average dip of 65.1 degrees.

211 The host rock, strike length, mean strike, mean dip, and minimum and maximum width of each vein
212 are summarized in Table 1.

213 The top and bottom surfaces of major quartz veins modelled in 3D (Fig. 4a) indicate that the
214 thickness of the veins decreases with depth and that the veins generally have a flaring upwards
215 geometry (Fig. 4b). The attitude of the modeled vein surfaces is generally different from that
216 observed in vein outcrops (compare Tables 1 and 2) since the veins change geometry with depth
217 (Fig. 4b). Histograms of the subsurface dip data of the modeled veins show that the dominant
218 subsurface dip angle of each vein is close to that measured at the surface. In addition, rose plots of
219 the subsurface strike data indicate that the dominant subsurface strike of each vein is close to that at
220 the surface (Table 1 and Fig. 4c), although there are not many measurements from the surface due to
221 erosion along vein walls (Table 1). The mapped variable geometry along strike is mirrored at depth

222 and most of the veins have multiple locations at depth where the dip changes (i.e. the veins have
223 vertically segmented sections with differing dips) (Fig. 4b). E-W trending veins have more geometric
224 irregularities than NE-SW trending ones both along strike and dip (Fig. 4c and Table 2: see standard
225 deviation values).

226 In layered rocks such dip segmentation has been previously interpreted to be the result of the
227 competency contrast within different host rocks (e.g. Schopfer *et al.* 2006, 2007). However at this
228 site the dip segmentation appears to be independent of the host rock type. Segmentation in the dip
229 direction may also be caused by the growth and coalescence of small planar segments of the
230 structures (whether faults or open-mode fractures) (Cox 2005).

231

232 **Wall rock veins**

233

234 Detailed structural data (thickness, infill type, length, attitude, and typology) were collected from the
235 wall rock structures surrounding two of the major mineralized quartz veins: the Karatepe vein and
236 the Topyurt vein. Dense vegetation and thick soil cover around other vein-associated structures
237 prevented the collection of structural data.

238 The E-W trending Karatepe vein is associated with an array of extensional veins in the wall rock which
239 defines left-lateral kinematics (Fig. 5a). These veins have comb textured hydrothermal quartz crystals
240 oriented perpendicular to the vein walls (Fig. 5b-c). Their width varies between 4 cm and 26 cm.
241 Their orientations are given in Fig. 5d. The wall rock veins in drill core define a complex mesh of
242 multiple fracture orientations with mutual cross-cutting relationships (Fig. 6a-b) indicating several
243 episodes of fracturing in the damage zone to the main veins.

244 The Karatepe wall rock also contains veinlets that are too thin to be visible in hand specimen. The
245 petrographical studies showed that the veinlets are filled by inequant granular hydrothermal quartz
246 (Fig. 6c). This texture shows that the opening of the fracture was more rapid than the growth of the
247 quartz crystals (Ramsay 1980; Woodcock *et al.* 2007).

248 The area surrounding the Topyurt vein system is also dominated by extensional veins (Fig. 7a). These
249 veins are only observed in the FW of the Topyurt vein (the hangingwall is not exposed) (Fig. 7a) and
250 their width varies between 3 cm and 20 cm on the surface. They are characterized by the same infill
251 of hydrothermal quartz and have comb textured hydrothermal quartz crystals oriented perpendicular
252 to the vein walls (Fig. 7b). A stereonet of their orientation data is presented in Fig. 7c. The NE-SW

253 trending Topyurt vein components and its wall rock structures are consistent with a right-lateral en-
254 echelon brittle shear zone.

255

256 **Sheeted quartz veins**

257

258 Sheeted quartz veins hosting epithermal mineralisation are present along the Kestanelik River valley
259 in the southern part of the study area (Fig. 2). These closely-spaced, sub-vertical and sub-parallel
260 veins are oriented almost perpendicular to the course of the river bed, hosted by QFH porphyry (Fig.
261 8a) and comprise up to 25% of the total rock volume. Their thicknesses vary between 0.5 cm and 15
262 cm (Fig. 8b-c). They therefore cannot be shown individually on the map, and the region where they
263 crop out has been indicated by shading (Fig. 2). Although outcrop quality is variable across the area,
264 similar veins are seen nowhere else, so they appear to be confined to the deep levels of the vein
265 system where exposed in the deeply incised river valley.

266 These steeply dipping veins contain well-developed hydrothermal quartz crystals almost
267 perpendicular to the vein walls (Fig. 8c), and there is no evidence of shearing along the vein walls;
268 therefore they are very likely to be extensional veins. Attitude data recorded from these veins are
269 shown on a stereonet (Fig. 8d).

270

271 **Vein textures and breccias**

272

273 The epithermal quartz veins at the Kestanelik deposit are dominated by the textures resulting from
274 the boiling of hydrothermal fluids such as cockade (Fig. 9) and colloform (Fig. 10b) textures indicative
275 of open space filling characteristics, and textures representing replacement such as pseudo-bladed
276 and saccharoidal (e.g. Buchanan 1981; White & Hedenquist, 1990; Dong *et al.* 1995). Colloform
277 texture at Kestanelik refers to fine rhythmic bands of chalcedony (Fig. 10b). Cockade texture forms
278 when isolated fragments of wall rock or early vein material are rimmed by fine-grained rhythmic
279 bands of quartz (Figs 9, 10b). Pseudo-bladed texture forms when quartz or chalcedony aggregates
280 replace bladed or platy calcite along their original crystal outlines (Fig 11b-f-h) immediately after the
281 boiling and removal of CO₂. Saccharoidal texture occurs when quartz replaces the massive granular

282 carbonate along crystallographic defects, and in this texture, loosely packed vitreous to milky fine
283 grained quartz aggregates show sugar appearance in hand specimen (Figs 11a-d-e, 12).

284 Although the Karatepe vein is dominated by chalcedony, other veins are characterized by quartz
285 infill. The most striking feature of the veins is brecciation suggesting multiple generations of
286 hydrothermal fluid flow and mineralisation. All the major veins are brecciated except the Karatepe
287 vein (Table 1). The sheeted veins are not brecciated, though they can display two different
288 generations of fills (Fig. 8c).

289 The Karatepe vein is dominated by breccias with cockade texture hosted by altered QFH porphyry.
290 Wall rock clasts within the cockade breccia are sub-rounded to rounded and poorly sorted. This
291 shows that the vein was emplaced along a zone that was already brecciated before the first phase of
292 fluid flow. The clasts show neither normal nor reverse grading in any of the drill cores from all depths
293 of the vein, (Fig. 9).

294 A cataclasite of feldspar (from the wall rock QFH porphyry) and early chalcedony (Fig. 10a) cemented
295 by a relatively later (younger) phase of chalcedony was observed by the petrographic study of thin
296 section from a drill core sample (Fig. 10b) taken from the FW of the Karatepe vein-wall rock contact.
297 This cataclasite indicates that after the vein was sealed due to a first phase of fluid flow and
298 associated mineralisation, further shearing occurred along vein FW-wall rock contact, producing
299 cohesive cataclasite.

300 All veins except the Karatepe vein are cement supported, monomictic to polymictic breccias
301 composed mostly of clasts derived from host rocks mainly schist and/or pre-existing quartz veins
302 cemented by quartz or quartz-iron-oxide (hematite and/or goethite or both). Four different breccia
303 types were recognized on the basis of macroscopic and microscopic observations from the vein
304 outcrops and drill cores; **(1) Cement-supported breccias**, comprising host rock clasts, most commonly
305 schist, cemented either by saccharoidal or pseudobladed quartz, or by crystalline quartz. The poorly-
306 to well-sorted clasts are angular to sub-angular, and the cement is more than 50% of the rock
307 volume. These breccias are generally observed close to the vein margins and form semi-continuous
308 domains on the exposed vein outcrops (Fig. 11a-b). Schist clasts commonly have silicification
309 between foliation planes. In Fig. 11c, foliation-parallel silicification is synchronous with the silica
310 forming the breccia cement: silica at the contact of the clast with the cement can be seen to be in
311 optical continuity with the foliation-parallel silica. Conversely, in Fig. 11d, clasts containing foliation-
312 parallel silicification are surrounded by a later quartz cement. **(2) Crackle (jigsaw-fit) breccias**,
313 consisting of clasts of pre-existing vein infill that generally match together and are cemented by
314 quartz-hematite or quartz- goethite in a network of veinlets. Moderately- to well-sorted clasts are

315 generally angular to sub-angular. In these cement-supported breccias, the cement is always less than
316 50% of the rock volume (Fig. 11e-f-g). **(3) Chaotic breccias** are composed of polymictic clasts of host
317 rock and/or pre-existing vein infill with different quartz textures. The cement is quartz-hematite or
318 quartz-goethite. Clasts are sub-angular to angular, poorly- to well-sorted, and range from mm to cm
319 scale. These breccias are generally more frequent at the highest part of the vein outcrops (Fig. 11h-i).
320 **(4) Tectonic breccias** with shear indicators were only seen in two different thin sections made from
321 K3 vein and provides evidence that the E-W trending K3 vein was originally a fault. Deformed clasts
322 and grains of saccharoidal quartz belonging to the previous phase have a cement of micro- to
323 crystalline quartz-hematite. They were only observed in thin sections made from the samples taken
324 from the margin of the K3W vein FW (Fig. 11j). Tectonic breccia has not been observed at the field
325 scale – only in thin section. This may be because subsequent hydrothermal brecciation overprints any
326 tectonic breccias formed during earlier shearing.

327

328 **Host rock deformation**

329

330 The Karatepe, K3E and Topyurt veins are hosted by QFH porphyry, while the other veins are hosted
331 by schist. Deformation of the wall rock hosting each vein was studied in the field and drill core, and is
332 summarized in Table 3. An important observation is that no shear indicator such as slickenlines was
333 seen in the field at the Karatepe vein boundary.

334 Host rock schist around the NE-SW trending KK1, KK2, KK3, KK4 and K1 veins does not change
335 foliation orientation adjacent to the veins and these veins have very sharp contacts with their host
336 rock schist as observed in the field and drill cores (Fig. 12). In addition, drillcore and grab samples
337 taken from the vein-wall rock contact do not return any shear indicator in petrographic analyses.

338 In contrast, the schist around the E-W trending K2 vein is highly fractured, contains hydrothermal
339 quartz veins up to 6-7 cm wide that are discordant to the foliation planes, while the foliation can be
340 observed to bend into the vein (Fig. 13a). In drill cores the wall rock schist of the K3 vein is also
341 intensely fractured and brecciated (Fig. 13b-c). In addition, tectonic breccia with deformed clasts and
342 grains of vein rock was observed at the vein footwall-wall rock contact (Fig. 11j) in the petrographic
343 analyses.

344 The E-W striking Karatepe vein, hosted by porphyry, is surrounded by a domain of cemented
345 extensional fractures and a small-scale post-mineralisation fault with small displacement

346 (approximately 1 meter) on the Karatepe vein (Fig. 5). Cataclasite is also found at the vein footwall-
347 wall rock contact (Fig. 10) in the petrographic analyses, which is an important shear indicator.

348 The wall rock zone of the Topyurt vein is also intensely deformed with many extensional veins and
349 hard-silicified resistant porphyry screens (Fig. 7).

350

351 **Discussion**

352

353 **Kinematics of the vein system**

354

355 Cataclasite at the margin of the Karatepe vein (of feldspar from wall rock QFH, and chalcedony from
356 first phase of mineralisation) contains asymmetric shear indicators (Fig. 10a), suggesting that the
357 structure hosting the vein is a fault. Hydrothermal quartz forming the Karatepe vein (Fig. 9) and filling
358 the comb fractures around it (Fig. 5c) shows that these structures are formed within the same
359 deformation event. Infill of a comb quartz veinlet adjacent to the Karatepe vein has a granular
360 texture and inequant fabric rather than a fibrous texture (Fig. 6c), which shows that the opening of
361 the fracture was more rapid than the growth of the quartz crystals. We suggest that the brittle
362 fracturing and dilation occurred during co-seismic or post-seismic aftershock phases of an
363 earthquake, and then quartz cement was deposited progressively and sealed the fracture during the
364 passive interseismic phase (e.g. Ramsay 1980; Woodcock *et al.* 2007). Furthermore, comb textured
365 extension fractures around the Karatepe vein are proximal to the vein margin (Fig. 5b-c), and most of
366 them curve towards the vein. This suggests that they are extensional fractures adjacent to the
367 Karatepe fault that formed after slip on the irregular Karatepe fault plane.

368 The Karatepe fault-hosted vein is surrounded by extensional veins that have orientations consistent
369 with left-lateral kinematics. We can infer a palaeostress for this subset of structures by assuming that
370 the minor principal stress is perpendicular to the mean orientation of the Karatepe damage zone
371 extensional veins, and their intersection with the fault plane is parallel to intermediate principal
372 stress. The results of these calculations gives orientations of σ_1 , σ_2 and σ_3 of **034°/02°, 124°/59° and**
373 **304°/31°** respectively (Fig. 14a-b). Hydrothermal macro crystalline quartz was also observed also in
374 the extensional veins along the river valley similar to the ones around the Topyurt and Karatepe
375 veins. The consistent textures and orientations of the main veins and sheeted veins suggest that all

376 these veins are related to same hydrothermal mineralization event. Strikes of all these veins (Fig.
377 14c) suggest that the horizontal component of the minimum principal stress (σ_3) was **N35°W**. The
378 Karatepe inferred stress (Fig. 14a) compares well with the extension direction for all the measured
379 extensional veins in the field area (Fig. 14c).

380 Similar analyses cannot be conducted for K2 and K3 veins. Although the drill cores show that K2 and
381 K3 have extensional veins in the damage zone, they are not exposed at the surface, so their
382 orientations cannot be measured. The K2 and K3 veins are dipping to the north, opposite to
383 Karatepe, but if they were active in the same stress field they too would have a component of left-
384 lateral slip. In the absence of a more complete dataset (for instance through oriented drill core) it is
385 not possible to conduct a more sophisticated paleostress analysis, but the structures all seem
386 consistent with subhorizontal NE-SW σ_1 .

387 The tilt on the younger sediments means that the older veins must also have been tilted. However it
388 is not straightforward to relate untilted stress orientations to tectonics because (1) as there may be
389 unmapped faults which tilt different blocks in the younger sediments, (2) previous tilting may have
390 affected the block of mineralized veins before the formation of the unconformity and (3) Late
391 Miocene aged vertical axis rotations (Kaymakci *et al.* 2007) must also be considered for re-
392 constructing the paleo-stresses responsible for the geothermal system, although the amount of such
393 vertical axis rotations are very difficult to constrain because of the large error ranges in the
394 palaeomagnetic measurements. Instead we want to establish if the vein sets are consistent with
395 formation in a single stress regime.

396 The inferred directions of the principal stresses indicate that the E-W trending Karatepe, K3 and K2
397 veins can be characterized as left lateral strike-slip faults, while NE-SW trending KK1, KK2, KK3, KK4
398 and K1 veins are extensional (Mode I) fractures (Figs 14d-e, 15). In addition, the NE-SW trending
399 Topyurt vein and associated N-S trending zone of wall rock veins correspond to a right lateral en-
400 echelon brittle shear zone (Fig. 14d-e). Although kinematic indicators could not be found for the
401 fault-hosted veins, sheared cataclasite, tectonic breccia and intensely deformed characteristics of the
402 wall rocks suggest that they are developed as a result of shearing. However, the NE-SW trending KK1,
403 KK2, KK3, KK4 and K1 veins do contain evidence of extensional fracturing (Mode I opening) and lack
404 any shear indicators and wall rock deformation.

405

406 **Permeability enhancement and fluid flow**

407

408 Integration of the data from the Kestanelik epithermal vein system and the review of the literature
409 suggest that three permeability enhancement and fluid flow mechanisms that could have been active
410 in the Kestanelik epithermal gold deposit.

411

412 *Co-seismic rupturing*

413 Co-seismic rupturing generates permeable pathways, which are clogged progressively by interseismic
414 hydrothermal sealing. Sibson (1987) suggested that episodic fault rupture causes co-seismic dilation
415 at the rupture zones and an associated fluid pressure drop. The co-seismic fluid pressure drop drives
416 boiling, which is evidenced by the common occurrence of pseudo-bladed quartz and crackle breccia
417 in the Kestanelik veins. Rapid closure of permeability by hydrothermal precipitation clogs pathways
418 and results in local pressure build-up. Quartz-iron oxide cement within the breccias shows that
419 ascending boiled fluid may also have mixed with descending oxidized surface meteoric water in the
420 shallower parts of the system (Fig. 15). Salinity and homogenization temperature data from fluid
421 inclusion analyses along with the O- and H- stable isotope analyses of fluid inclusions could be used
422 to further constrain boiling and mixing events.

423 Shear indicators such as cataclasite and tectonic breccia cemented by a later phase of silicification
424 are observed at the footwall of the vein-wall rock contacts of the Kestanelik fault-hosted veins. These
425 and the presence of angular wall rock clasts at the margins of extensional (Mode I) fractures suggest
426 rupturing along the fault planes and extensional fractures (Fig. 15).

427 The inequigranular infill of a comb quartz veinlet at the wall rock of the Karatepe vein shows that the
428 opening of the fracture was more rapid than the growing of the quartz crystals. This texture is more
429 consistent with the brittle fracturing and dilation occurring during co-seismic or post-seismic
430 aftershock phases of an earthquake, than with progressive silicification to seal the fracture during the
431 passive interseismic phase (Woodcock *et al.* 2007). In addition, the absence of any grading in the
432 clasts of the cockade breccias of the Karatepe vein (Fig. 9) may indicate that both shaking (where
433 brecciation occurs due to seismic faulting and clasts are cemented during interseismic period) and
434 fluidisation (see below) may have played a role in the formation of the cockade breccias (c.f. Frenzel
435 & Woodcock 2014): These represent the first phase of fluid flow and formation of the Karatepe vein.

436

437 *Hydraulic fracturing*

438

439 Rapid hydrothermal sealing of the pathways by mineral deposition could cause an increase in
440 hydrothermal fluid pressure. Increase in fluid pressure may promote extensional-shear failure of the
441 vein walls at depth, which are subsequently propagated upwards into the shallowest part of the
442 crust. Provided that the pore fluid factor increases at rates higher than the increase in stress
443 difference (Cox 2005), when the hydrothermal fluid pressure exceeds the combined minimum
444 principal stress (σ_3) and the tensile strength of the cap rock (T), then hydraulic fracturing occurs
445 (Phillips 1972). This triggers boiling due to pressure release and creates permeable structural
446 conduits for the input of fluids, and results in formation of hydrothermal crackle breccias without
447 significant rotation of the fragments (Jebrak 1997). The cements have to be very rapidly deposited or
448 the clasts would settle out causing grading and/or rotation. Crackle breccias with fragments of the
449 early quartz infill without significant rotation cemented by later quartz or quartz iron-oxide-forming a
450 network of veinlets observed at Kestanelik veins (Fig. 11e-f-g) indicate dilatant fracturing with a
451 negligible shear component and suggest hydraulic fracturing may have occurred at the main vein
452 conduits. As discussed above, the absence of any grading may indicate fluidisation, where brecciation
453 occurs due to hydraulic fracturing and subsequent fluid flow cements the clasts (Frenzel & Woodcock
454 2014)

455

456 *Transient local stress variation*

457

458 Local stress orientation can change transiently, resulting in permeability enhancement. Intrusion of
459 dykes coeval with the gold mineralisation at Kestanelik (Fig. 3), and the dynamic nature of the
460 geothermal systems may explain the transient kinematic variation by disrupting the local stress field
461 and triggering earthquakes (Fukuyama *et al.* 2001; Toda *et al.* 2002; Waite & Smith 2002;
462 Micklethwaite 2009). Transient local stress variation might enhance permeability along the
463 corrugated strike of the Kestanelik structures by facilitating slip on misoriented surfaces and
464 influencing the kinematics of the structures. In addition, locations where the dip changes in the
465 Kestanelik structures have potential to enhance permeability since they lead to stress concentrations
466 and localize intense deformation compared to the smooth and planar segments (Cox 2005) during
467 the earthquakes. It is important to note that permeability and fluid flow will be intermittent in both
468 cases.

469

470 **Conceptual model for the evolution of the Kestanelik veins**

471

472 On the basis of field, drill hole and microstructural observations we suggest that the dominant
473 mechanism for formation of the vein textures was co-seismic ruting (Figure 15). When an
474 earthquake occurred, E-W trending fault-hosted veins reactivated and opened along their footwall-
475 wall rock contacts. Conversely NE-SW trending mode I fracture-hosted veins reactivated and opened
476 along either margin. Coseismic rupture and dilation resulted in rapid fluid pressure drop and drove
477 boiling of hydrothermal fluids. Boiling fluid rose along the newly created permeable pathways and
478 may have mixed with descending oxidized surface meteoric water at the shallower parts of the
479 system. The evidence for rupture along the walls of the veins includes: shear indicators such as
480 cataclasite and tectonic breccia of wall rock; pre-existing vein infill cemented by a later phase of
481 silicification observed at the footwall of the vein-wall rock contacts of the two of the fault hosted
482 veins (Karatepe and K3 veins), and the presence of angular wall rock clasts at the margins of
483 extensional (Mode I) fractures. Evidence for multiple brecciation and sealing events is chaotic
484 breccias with polymictic clasts from pre-existing vein infill and clasts of wall rock cemented by quartz-
485 hematite or quartz-goethite. This evidence suggests repeated reactivation and opening in
486 subsequent co-seismic events. Crackle breccias are evidence that hydraulic fracturing may also have
487 taken place.

488 Although none of the fault rock textures that have been observed are definitely diagnostic of
489 dynamic rupture, it is not possible to exclude dynamic slip (Cowan, 1999; Rowe & Griffith 2015).
490 However it has been documented that earthquake rupturing can induce opening of faults and
491 fractures off the plane of the main fault (Micklethwaite & Cox 2004, 2006). Kestanelik was likely to
492 have been an earthquake prone region in the Late Eocene at the time of mineralisation because of
493 the tectonic activity caused by further convergence after the closure of the northern branch of the
494 Neo-Tethys Ocean (Late Cretaceous-Early Eocene: Şengor & Yılmaz 1981; Okay & Tüysüz, 1999;
495 Sherlock *et al.* 1999; Önen & Hall 2000; Kaymakci *et al.* 2007, 2009). In addition, it is well known that
496 geothermal regions are dynamic, and that pressure transfer due to hydrothermal flow and
497 mineralisation can induce seismicity (e.g. Hill 1977).

498 As noted above, the altered porphyry zone is wider than usually expected for structurally-controlled
499 alteration. It is possible that this wide halo is further evidence for multiple recharge events of the
500 altering fluids through repeated rupture of the main veins, and more protracted flow within the
501 damage zone veins.

502

503 **Implications for prospect evaluation**

504

505 Mapping and study of veins, wall rock veins and collecting structural data on the veins are powerful
506 tools to unravel the kinematics of the vein system. Correlation of the kinematics of the mineralized
507 or high-grade vein system along with timing of the mineralisation may help to discover the areas or
508 targets by defining the favourable orientation for structures to the mineralisation. Because repeated
509 boiling results in multiple overprinting of textures, key features such as the shear textures may be
510 missed if only a limited number of outcrop or drill cores are examined; therefore comprehensive
511 petrographic investigation of vein material and delineating the ore-vein textures addressing multiple
512 boiling and silicification phases (especially close to the vein margins) is strongly advised. The
513 understanding of textures showing clogging and subsequent boiling of the hydrothermal systems in
514 correlation with structural easement or enhancement of fluid flow along the conduits may contribute
515 to the target assessment in epithermal systems as gold precipitation is triggered by boiling and
516 oxidation in low sulphidation epithermal gold deposits. Thus mapping and petrographical analysis of
517 the ore-vein textures both on the outcrops and in drillcores together with the geochemical analysis
518 of gold assay data not only help to understand the likely gold deposition mechanism(s) but also the
519 potential gold distribution within the deposits.

520

521 **Conclusions**

522

523 The Kestanelik fracture system is a LS epithermal gold deposit evident from pseudo-bladed quartz,
524 colloform to crustiform quartz, comb to cockade ore-vein textures, and hydrothermal breccias. The
525 mineralisation is hosted by major quartz veins up to 13.6 m thick, as well as sheeted extensional
526 quartz veins in the valley and, extensional wall rock veins surrounding the major quartz veins. Vein
527 textures and breccias are indicative of repeated sealing and subsequent brecciation of wall rock and
528 the pre-existing vein infill. Boiling and fluid mixing are likely mechanisms of gold deposition.
529 According to the field and petrographic data; the kinematics of the vein system is consistent with
530 formation in a single regional stress field: E-W trending veins are characterized as left lateral faults,
531 whilst NE-SW trending veins are characterized as extensional (Mode I) fractures. The gold grade is
532 higher in the extensional veins; although further detailed analysis of the vein textures is required to
533 unpick the mechanism(s) of gold deposition.

534 Cataclastic deformation and tectonic brecciation of wall rocks and early quartz, hydrothermal crackle
535 breccias, and matrix supported chaotic breccias of pre-existing vein infill, all of which are cemented
536 by late iron-oxide-bearing quartz indicate that co-seismic rupturing and hydraulic fracturing are two
537 major permeability enhancement mechanisms which would have caused repeated reactivation of
538 clogged permeable pathways at Kestanelik. Additionally, transient local stress variation, caused by
539 syn-mineralisation dyke intrusion, has the potential to enhance permeability on mis-oriented
540 surfaces and at locations where the dip changes on vein planes. These results indicate that a
541 thorough understanding of structural geology and kinematics, when coupled with the examination of
542 evidence for boiling and other mineralisation mechanisms should be an important tool in defining
543 ore zones within areas of mineralisation in epithermal gold deposits.

544 **Acknowledgements**

545 This work is a part of a Ph.D. study carried out at the University of Strathclyde with University of
546 Strathclyde scholarship and financial support of Geochemico Incorporated. John Cosgrove and
547 Steven Micklethwaite are thanked for their constructive reviews of the manuscript. The authors
548 acknowledge Chesser Resources for providing accommodation and logistics for fieldwork, and access
549 to the drill core data. We gratefully thank Cem S. Yüceer, Murat Çetintas, and geologists and staff at
550 Kestanelik for their generous help in all phases of the field work. We also would like to thank Prof.
551 Ercan Özcan for biostratigraphical age determinations of Eocene units.

552

553 **Funding information**

554 NG is grateful to the University of Strathclyde for funding the Ph.D. The authors are thankful to the
555 Geochemico Incorporated for financial support.

556

557 **References**

558 Allmendinger, R.W., Cardozo, N.C. & Fisher, D. 2013. *Structural Geology Algorithms: Vectors &*
559 *Tensors*. Cambridge University Press, Cambridge, 289.

560

561 Altunkaynak, Ş. & Genç, Ş.C. 2008. Petrogenesis and time-progressive evolution of the Cenozoic
562 continental volcanism in the Biga Peninsula, NW Anatolia (Turkey). *Lithos*, **102**, 316–340.

563

564 Buchanan, L.J. 1981. Precious metal deposits associated with volcanic environments in the
565 southwest. *In*: Dickson, W.R. & Payne, W.D. (eds) *Relations of Tectonics to Ore Deposits in the*
566 *Southern Cordillera*. Arizona Geological Society Digest, 14, 237-262.

567

568 Burnside, N.M., Shipton, Z.K., Dockrill, B. & Ellam, R.M. 2013. Man-made versus natural CO₂ leakage:
569 A 400 k.y. history of an analogue for engineered geological storage of CO₂. *Geology*, **41**, 471–474.

570

571 Caine, J., Evans, J., & Forster, C. 1996. Fault zone architecture and permeability structure. *Geology*,
572 **24**, 1025–1028.

573

574 Cardozo, N. & Allmendinger, R. W. 2013. Spherical projections with OSXStereonet: *Computers &*
575 *Geosciences*, **51**, no. 0, 193-205.

576

577 Cowan, D.S. 1999. Do faults preserve a record of seismic slip? A field geologist's opinion. *Journal of*
578 *Structural Geology*, **21**, 995-1001.

579

580 Cox, S., Knackstedt, M. & Braun, J. 2001. Principles of structural control on permeability and fluid
581 flow in hydrothermal systems. *Reviews in Economic Geology*, **14**, 1-24.

582

583 Cox, S. 2005. Coupling between Deformation, Fluid Pressures, and Fluid Flow in Ore-Producing
584 Hydrothermal Systems at Depth in the Crust. *Economic Geology*, **100**, 39-75.

585

586 Curewitz, D. & Karson, J.A. 1997. Structural settings of hydrothermal outflow: Fracture permeability
587 maintained by fault propagation and interaction. *Journal of Volcanology and Geothermal Research*,
588 **79**, 149–168.

589

590 Davatzes, N. C., Eichhubl, P. & Aydin, A. 2005. Structural evolution of fault zones in sandstone by
591 multiple deformation mechanisms: Moab fault, southeast Utah. *Geological Society of America*
592 *Bulletin*, **117**, 135–148.

593

594 Dong, G., Morrison, G. & Jaireth, S. 1995. Quartz textures in epithermal veins, Queensland—
595 classification, origin, and implication. *Economic Geology*, **90**, 1841–1856.

596

597 Fournier, R.O. 1989. Geochemistry and dynamics of the Yellowstone National Park hydrothermal
598 system. *Annual Review of Earth and Planetary Sciences*, **17**, 13–53.

599

600 Frenzel, M. & Woodcock, N.H. 2014. Cockade breccia: product of mineralisation along dilational
601 faults. *Journal of Structural Geology*, **68**, 194-206.

602

603 Fukuyama, E., Kubo, A., Kawai, H. & Nonomura, K. 2001. Seismic remote monitoring of stress field.
604 *Earth, Planets and Space*, **53**, 1021–1026.

605

606 Hedenquist, J.W. & Lowenstern, J.B. 1994. The role of magmas in the formation of hydrothermal ore
607 deposits. *Nature*, **370**, 519-527.

608

609 Sillitoe, R. H. & Hedenquist, J. W. 2003. *Linkages between volcanotectonic settings, ore-fluid*
610 *compositions, and epithermal precious metal deposits*. Society of Economic Geologists, Special
611 Publications, **10**.

612 Hedenquist, J.W. 2011. Observations on the Kestanelik and Karaayi prospects, Biga Peninsula, Turkey.
613 *Unpublished report for Chesser Resources Ltd.*, 24.

614

615 Hedenquist, J.W., Arribas M. A. & Gonzalez-Urien, E. 2000. Exploration for epithermal gold deposits.
616 *Reviews in Economic Geology*, **13**, 245-277.

617

618 Henley, R.W. 1985. The geothermal framework of epithermal deposits. *Reviews in Economic*
619 *Geology*, **2**, 1-24.

620

621 Hill, D.P. 1977. A model for earthquake swarms. *Journal of Geophysical Research*, **82**, 1347–1352.

622

623 Hulin, C.D. 1929. Structural control of ore deposition. *Economic Geology*, **24**, 15-49.

624

625 Janecke, S.U. & Evans, J.P. 1988. Feldspar-influenced rock rheologies. *Geology*, **16**, 1064- 1067.

626

627 Jébrak, M. 1997. Hydrothermal breccias in vein-type ore deposits: a review of mechanisms,
628 morphology and size distribution. *Ore Geology Reviews*, **12**, 111-134.
629

630 Kaymakci, N., Aldanmaz, E., Langereis, C., Spell, T.L., Gurer, O.F. & Zanetti, K.A. 2007. Late Miocene
631 transcurrent tectonics in NW Turkey: evidence from palaeomagnetism and ^{40}Ar – ^{39}Ar dating of
632 alkaline volcanic rocks. *Geological Magazine*, **144**, 379–392.
633

634 Kaymakci, N. Özcelik, Y. White, S.H. & Van Dijk, P.M. 2009. Tectono-stratigraphy of the Çankiri Basin:
635 Late Cretaceous to Early Miocene evolution of the Neotethyan Suture Zone in Turkey. In: Van
636 Hinsbergen, D.J.J., Edwards, M.A. & Govers, R. (eds) *Geodynamics of Collision and Collapse at the*
637 *Africa-Arabia-Eurasia subduction zone*, Geological Society, London, Special Publications, **311**, 67-106.
638

639 Lalou, C., Reyss, J.L., Brichet, E., Arnold, M., Thompson, G., Fouquet, Y. & Rona, P.A. 1993. New age
640 data for Mid-Atlantic Ridge hydrothermal sites: TAG and Snakepit geochronology revisited. *Journal of*
641 *Geophysical Research*, **98**, 9705-9713.
642

643 Micklethwaite, S. & Cox, S. 2004. Fault-segment rupture, aftershock-zone fluid flow, and
644 mineralisation. *Geology*, **32**, 813-816.
645

646 Micklethwaite, S. & Cox, S. 2006. Progressive fault triggering and fluid flow in aftershock domains:
647 Examples from mineralized Archean fault systems. *Earth and Planetary Science Letters*, **250**, 318-330.
648

649 Micklethwaite, S. 2009. Mechanisms of faulting and permeability enhancement during epithermal
650 mineralisation: Cracow goldfield, Australia. *Journal of Structural Geology*, **31**, 288-300.
651

652 Micklethwaite, S., Sheldon H.A. & Baker, T. 2010. Active fault and shear processes and their
653 implications for mineral deposit formation and discovery. *Journal of Structural Geology*, **32**, 151-165.
654

655 Okay, A.I. & Tüysüz, O. 1999. Tethyan sutures of northern Turkey. In: Durand B., Jolivet, L.,
656 Horváthand F. & Séranne, M. (eds) *The Mediterranean Basins: Tertiary extension within the Alpine*
657 *orogen*, Geological Society, London, Special Publications, **156**, 475-515.

658

659 Okay, A.I., Siyako, M. & Bürkan, K.A. 1990. Geology and tectonic evolution of the Biga Peninsula (in
660 Turkish). *Bulletin of the Turkish Association of Petroleum Geologists*, **2**, 83-121.

661

662 Okay, A.I., Satir, M., Maluski, H., Siyako, M., Monie, P., Metzger, R. & Akyüz S., 1996. Paleo- and Neo-
663 Tethyan events in northwest Turkey: geological and geochronological constraints. *In*: Yin, A. &
664 Harrison, M. (ed.) *Tectonics of Asia*, Cambridge University Press, Cambridge, 420-441.

665

666 Önen, P. & HALL, R. 1993. Ophiolites and related metamorphic rocks from the Kütahya region,
667 northwest Turkey. *Geological Journal*, **28**, 399-412.

668

669 Phillips, W. J. 1972. Hydraulic fracturing and mineralisation: *Journal of the Geological Society of*
670 *London*, **128**, 337– 359.

671

672 Ramsay, J. 1980. The crack-seal mechanism of rock deformation. *Nature*, **284**, 135-139.

673

674 Rowe, C. D. & Griffith, W. A. 2015. Do faults preserve a record of seismic slip: A second opinion.
675 Invited Review, *Journal of Structural Geology*, **78**, 1-26.

676

677 Rowland, J.V. & Sibson, R.H. 2004. Structural controls on hydrothermal flow in a segmented rift
678 system, Taupo Volcanic Zone, New Zealand. *Geofluids*, **4**, 259–283.

679

680 Sanchez-Alfaro, P., Reich, M., Driesner, T., Cembrano, J., Arancibia, G., Perez-Flores, P., Heinrich, C.A.,
681 Rowland, J., Tardani, D., Lange, D. & Campos, E. 2016. The optimal windows for seismically-enhanced
682 gold precipitation in the epithermal environment. *Ore Geology Reviews*, **79**, 463-473.

683

684 Schöpfer, M.P.J., Childs, C. & Walsh, J.J. 2006. Localisation of normal faults in multilayer sequences.
685 *Journal of Structural Geology*, **28**, 816-833.

686

687 Schöpfer, M.P.J., Childs, C., Walsh, J.J., Manzocchi, T. & Koyi, H.A. 2007. Geometrical analysis of the
688 refraction and segmentation of normal faults in periodically layered sequences. *Journal of Structural*
689 *Geology*, **29**, 318-335.

690

691 Şengör, A.M.C. & Yilmaz, Y. 1981. Tethyan Evolution of Turkey: A Plate Tectonic Approach.
692 *Tectonophysics*, **75**, 181-241.

693

694 Sherlock, S., Kelley, S., Inger, S., Harris, N. & Okay, A.I., 1999. ^{40}Ar - ^{39}Ar and Rb/Sr geochronology of
695 high-pressure metamorphism and exhumation history of the Tavsanli Zone, NW Turkey.
696 *Contributions to Mineralogy and Petrology*, **137**, 46-58.

697

698 Sibson, R.H. 1987. Earthquake rupturing as a mineralizing agent in hydrothermal systems. *Geology*,
699 **15**, 701–704.

700

701 Sillitoe, R.H., 2000. Porphyry copper systems. *Economic Geology*, **105**, 3–41.

702

703 Simmons, S. F., White, N. C. & John, D. 2005. Geological characteristics of epithermal precious and
704 base metal deposits: *Economic Geology 100th Anniversary Volume*, 485-522.

705

706 Spurr, J. E. 1925. Ore magmas versus magmatic waters. *Engineering and Mining Journal*, **119**, 890.

707

708 Toda, S., Stein, R. S. & Sagiya, T. 2002. Evidence from the AD 2000 Izu islands earthquake swarm that
709 stressing rate governs seismicity. *Nature*, **419**, 58–61.

710

711 Türkecan, A. & Yurtsever, A. 2002. *1:500 000 scale geological map of Turkey, İstanbul sheet*. General
712 Directorate of Mineral Research and Exploration publications, Ankara.

713

714 Ünal-İmer, E., Gulec, N., Kuscu, I. & Fallick, A.E. 2013. Genetic investigation and comparison of
715 Kartaldag and Madendag epithermal gold deposits in Canakkale, NW Turkey. *Ore Geology Reviews*,
716 **53**, 204-222.

717

718 Waite, G.P. & Smith, R.B., 2002. Seismic evidence for fluid migration accompanying subsidence of the
719 Yellowstone caldera. *Journal of Geophysical Research*, **107**, 2177.

720

721 White, N.C. & Hedenquist, J.W. 1990. Epithermal environments and styles of mineralisation:
722 Variations and their causes, and guidelines for exploration. *Journal of Geochemical Exploration*, **36**,
723 445–474.

724

725 White, N.C. & Hedenquist, J.W. 1995. Epithermal gold deposits: Styles, characteristics and
726 exploration. *Society of Economic Geologists Newsletter*, **23**, 9–13.

727

728 Woodcock, N.H., Dickson, J.A.D. & Tarasewicz, J.P. 2007. Transient permeability and reseal hardening
729 in fault zones: evidence from dilation breccia textures. *In*: Lonergan, L., Jolley, R.J.H., Rawnsley, K. &
730 Sanderson, D.J. (eds) *Fractured Reservoirs*, Geological Society, London, Special Publications, **270**, 43–
731 53.

732

733 **Figure captions**

734

735 **Fig. 1. (a)** Major tectonic divisions of Turkey (simplified from Okay & Tuysuz 1999). **(b)** Simplified
736 geological map of the Biga Peninsula with the location of the study area (modified from Türkecan &
737 Yurtsever 2002).

738

739 **Fig. 2.** Geological map of the study area Kestanelik deposit.

740

741 **Fig. 3.** A drillcore (KED-6 65.5–65.7 m) photo showing a mafic dyke (upper right) and adjacent breccia
742 with fragments of dyke and quartz vein cemented by quartz (upper left) on the margin of altered
743 QFH porphyry intruded by the dyke (bottom) indicating contemporaneous mineralisation and dyke
744 intrusion.

745

746 **Fig. 4. (a)** 3D view of modeled top and bottom surfaces of major quartz veins with DEM (Digital
747 Elevation Model). **(b)** Representative cross section of each vein showing the flaring upwards
748 geometry of the veins and their decreasing thickness with depth. **(c)** Rose plot of strike values and
749 histogram of dip amount values of HW surfaces of each vein showing the strike and dip variability of
750 modeled surfaces.

751

752 **Fig. 5. (a)** Detailed map of the Karatepe vein and its wall rock veins. **(b)** Photo showing one of the
753 extension veins around the Karatepe vein. **(c)** Closer view of the extension vein having comb textured
754 hydrothermal quartz. **(d)** Poles to the extensional veins around the Karatepe vein plotted on an
755 equal-area stereonet with the arrows indicating the opening direction for the veins.

756

757 **Fig. 6. (a)** A core sample from KED-18 133.8-134 m showing mutual cross-cutting relationships of the
758 wall rock veins close to the Karatepe vein footwall-wall rock contact (1.2 m from the vein wall down-
759 hole equivalent to 0.9 m perpendicular distance) at the FW of the vein. n.b. the host porphyry here is
760 not as altered as it is higher in the section where it has a strong yellow alteration (Fig. 5). **(b)** Sketch
761 of the core sample. **(c)** A comb quartz veinlet filled by inequant granular hydrothermal quartz, and
762 thinner quartz veinlets traversing the clay altered wall rock QFH porphyry close to the Karatepe vein
763 footwall margin showing that opening rate of the fracture > precipitation rate of the cement (cmb
764 qtz: comb quartz, wr: wall rock) (KED-16 124.4 m) (crossed polars image).

765

766 **Fig. 7. (a)** Detailed map of the Topyurt vein and its wall rock veins. **(b)** Photo showing one of the
767 extension veins having comb textured hydrothermal quartz around the Topyurt vein. **(c)** Poles to the
768 extensional veins around the Topyurt vein plotted on an equal-area stereonet with the arrows
769 indicating the opening direction for the veins.

770

771 **Fig. 8. (a)** Photo showing the sub-vertical and sub-parallel sheeted quartz veins along the Kestanelik
772 River valley. **(b)** Photo showing some of the sheeted quartz veins. **(c)** Closer view of one of the
773 sheeted extensional veins having comb textured well developed hydrothermal quartz crystals
774 oriented perpendicular to the vein walls. **(d)** Poles to the sheeted quartz veins plotted on an equal-
775 area stereonet with the arrows indicating the opening direction for the veins.

776

777 **Fig. 9.** Cockade breccias composed of chalcedony enclosing sub-rounded to rounded and poorly
778 sorted clay altered QFH porphyry clasts at different levels of the Karatepe vein. Size of individual
779 cockade breccias neither decreases nor increases as elevation decreases (Note that the scale is same
780 for each photo).

781

782 **Fig. 10. (a)** Cataclasite of feldspar (from the wall rock QFH porphyry) and early (phase 1) chalcedony
783 (crossed polars image). n.b. drill cores are not oriented so it is not possible to derive sense of slip. **(b)**
784 Photo of the drill core sample (KED-16 at 124.2-124.4 m) taken from the footwall of the Karatepe
785 vein-wall rock contact showing the thin section location in which cataclasite observed and two
786 different textures representing two different mineralization phases of the vein (fld: feldspar, ch:
787 chalcedony, col ch: colloform chalcedony, coc ch: cockade chalcedony, wr: wall rock).

788

789 **Fig. 11. (a)** Breccia with the clasts of wall rock schist plus a cement of saccharoidal quartz close to the
790 HW of the KK1 vein. **(b)** Breccia with the clasts of wall rock schist plus a cement of pseudo-bladed
791 quartz close to the HW of the KK2 vein. **(c)** Breccia with schist clast (note the silicification is after
792 brecciation, matrix and foliation planes are in optical continuity) (K3 vein) (crossed polars image). **(d)**
793 Comb quartz matrix between two clasts of silicified schist. Silicification is parallel to foliation and
794 before comb qtz formation. (KK1 vein) (crossed polars image). **(e)** Crackle breccia with the clasts of
795 saccharoidal quartz separated by quartz-hematite cement observed close to the margin of KK1 vein.
796 **(f)** Crackle breccia with the clasts of pseudo-bladed quartz separated by quartz-goethite cement

797 observed in a drillcore cutting the K3 vein (KED-14 70.5-70.65 m). (g) Crackle breccia with the clasts
798 of saccharoidal quartz cemented by quartz-goethite in a drillcore cutting the KK1 vein (KED-7 13.1-
799 13.2 m) (h) Chaotic breccia composed of polymictic clasts of pre-existing vein infill with different
800 quartz textures cemented by quartz-hematite in a drillcore cutting the K3 vein (KED-20 30.1-30.2 m).
801 (i) Chaotic breccia composed of polymictic clasts of pre-existing vein infill with different quartz
802 textures cemented by quartz-hematite from the upper levels of K3 vein outcrop. (j) Tectonic breccia
803 with deformed clasts and grains of early saccharoidal quartz which set in a microcrystalline quartz
804 matrix observed in a thin section made from a hand sample taken from the outcrop of the K3 vein
805 footwall margin (Note that the microcrystalline quartz replaces saccharoidal quartz fragments along
806 the microfractures) (crossed polars image). (sac qtz: saccharoidal quartz, psbld: pseudo-bladed
807 quartz, wr: wall rock, mqz: microcrystalline quartz, sil sch: silicified schist, cmb sac qtz: comb textured
808 saccharoidal quartz, goet: goethite, qtz-hem: quartz-hematite, qtz-goet: quartz-goethite).

809

810 **Fig. 12. (a)** Sharp contact between the footwall of the KK1 vein and wall rock schist. **(b)** Photo of KED-
811 105 74.5-82 m interval core boxes showing that the foliation of the schist does not change around
812 the K1 vein. Note that the white veins around the K1 vein interval generally observed parallel to the
813 foliation planes include meta-quartz. (Yellow dashed lines envelopes the vein interval).

814

815 **Fig. 13. (a)** Photo showing that the schist adjacent to the K2 vein is highly deformed and hosts
816 hydrothermal quartz veins discordant to the foliation planes (Waved black lines represent the
817 orientation of foliation surfaces; black dashed lines represent the boundaries of discordant veins.)
818 Note that the foliation surfaces are not continuous and change their attitude. **(b)** Photo of KED-76
819 78.5-86.2 m interval core boxes showing that the host rock porphyry is fractured, brecciated and
820 veined around the K3E vein. Note that porphyry includes the fragments of hydrothermal quartz
821 veinlets around the HW of the vein (Yellow dashed lines envelopes the vein interval). **(c)** Photo of
822 KED-20 24.9-33.4 m interval core boxes showing that the host rock schist is highly fractured and
823 brecciated around the K3W vein. Note that the deformation is higher around the HW of the vein and
824 schist includes the fragments of hydrothermal quartz veinlets around the HW of the vein (Yellow
825 dashed lines envelopes the vein interval).

826

827 **Fig. 14. (a)** Determination of principal stress orientations based on Anderson's theory of faulting by
828 plotting the plane representing the mean orientation of the Karatepe vein and the mean plane of the

829 adjacent extensional veins on an equal area stereonet based on assumptions: (1) Minor principal
 830 stress (σ_3) is perpendicular to the extensional veins (2) Their intersection with the fault plane is
 831 parallel to intermediate principal stress (σ_2). **(b)** A hypothethic diagram showing the relationship
 832 between the principle stress directions and opening of the veins and movement along the fault plane
 833 (M plane is the movement plane). **(c)** Poles to the all extensional veins in the Kestanelik deposit
 834 plotted on an equal-area stereonet with the arrows indicating the opening direction for the veins.
 835 **(d)** A sketch model showing the kinematics of the major quartz veins at Kestanelik based on the
 836 determined principal stress directions. **(e)** A hypothethical model showing the opening of the
 837 structures hosting the Kestanelik major quartz veins.

838

839 **Fig. 15.** A conceptual model for the repeated reactivation and opening of clogged veins and
 840 associated fluid flow, mineralisation and resulting vein textures at Kestanelik. Note that K3 vein
 841 represents the fault hosted veins (except Karatepe vein), while K1 vein represents the extensional
 842 (Mode I) fracture hosted veins of the Kestanelik.

843

844 **Tables**

845

846 **Table 1.** *General characteristics of major quartz veins. All data are from measurements in outcrop.*

Vein	Host rock	No of data	Mean strike	Mean dip	Dip direction	Strike length	Min. width (m)	Max. width (m)
Karatepe	QFH porphyry	23	084,2	69,8	SSE	350	0,8	8
KK1	schist	11	047,3	76,7	SE	150	1,2	9
KK2	schist	13	044,5	75,8	SE	185	1	8,5
KK3	schist	5	046,9	70,2	SE	52	2	8,7
KK4	schist	4	042,4	68,3	SE	47	1	5,8
K1	schist	15	039,6	75,1	SE	240	0,9	13,6
K2	schist	8	268	43,5	NNW	86	0,6	12,9
K3E	QFH porphyry	18	274,5	71	NNE	280	0,6	7,8
K3W	schist	16	237,3	62,3	NW	230	2	12,5
Topyurt	QFH porphyry	10	224,5	65,1	NW	154	2	10

847

848

849
850

Table 2. Descriptive statistics of modeled surfaces of each vein. All data are from the vertices of the subsurfaces).

Vein	Subsurface*	No of vertices	Mean		Standard deviation		Median		Average gold grade (g/t) †
			strike	dip	strike	dip	strike	dip	
Karatepe	FW	110847	91.9	55.9	26.3	8.5	85.8	56.3	0.461
	HW	26048	92.7	55.8	25.1	10.9	85.8	57.3	
KK1	FW	7019	56.5	60.4	13.5	6.5	54.8	59.1	3.356
	HW	6202	55	62.6	6.4	5.1	54.9	61.8	
KK2	FW	444923	65.7	51.8	11.8	4.6	66.3	52.1	2.081
	HW	341583	67.5	53.2	16.4	8.6	65.8	55.8	
KK3	FW	45065	65.1	61.1	16.5	3.9	65.3	61.6	3.484
	HW	52235	55.7	66.2	9	4.1	55.7	66.2	
KK4	FW	231999	56.6	57.5	7.9	3.8	56.8	58.3	0.866
	HW	209578	58.3	59.9	5.2	3	58.4	60.5	
K1	FW	502776	52.9	63.6	22.8	6.8	50.3	64.7	2.921
	HW	384859	52.9	67.5	19.8	7.6	49	68.7	
K3E	FW	1048569	261.9	66.4	29	17	264.9	70.2	1.326
	HW	1042016	261	69	29.6	16.6	266.1	72.4	
K3W	FW	439652	225.9	63.3	31.9	8	232.3	64.4	6.943
	HW	317971	227.8	64.5	31.3	8.9	234.1	66.4	

851 *FW: Footwall, HW: Hangingwall. As is common in the mining literature we use these terms to refer
852 to the wall below and above the vein respectively, and not to infer kinematics.

853 † Average gold grade values are calculated based on the geochemical gold assay data from the drill
854 cores of the modeled veins.

855

856

857

858

859

860

861

862

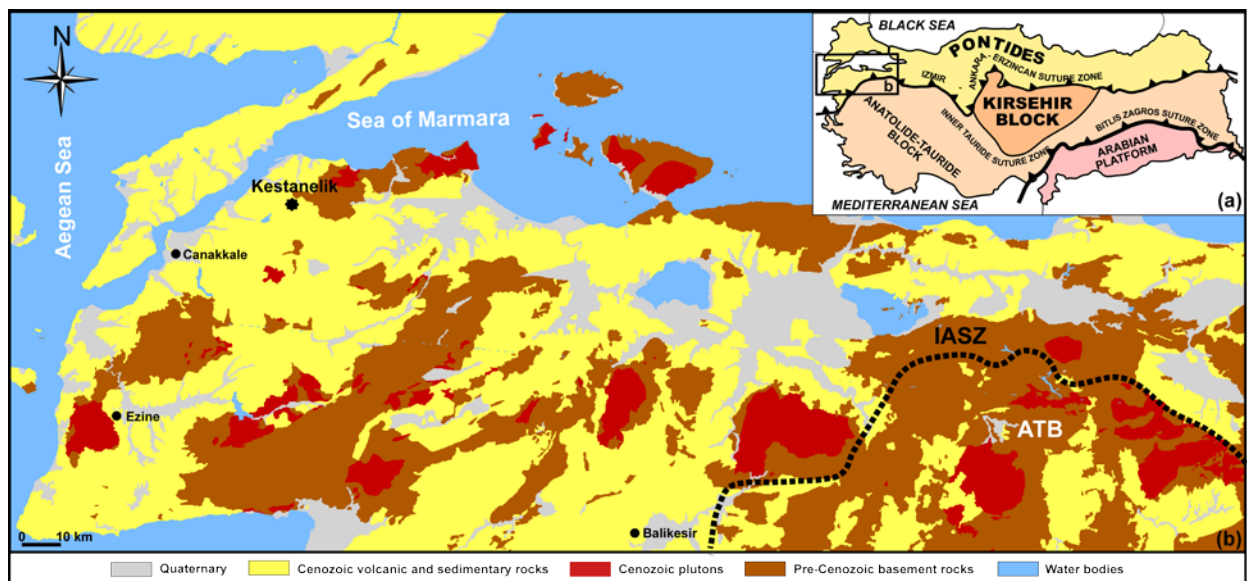
863 **Table 3.** Summary of host rock deformation observed around the major quartz veins.

Vein	Host rock	Host rock deformation*
Karatepe	porphyry	F, V
KK1	schist	ND
KK2	schist	ND
KK3	schist	ND
KK4	schist	ND
K1	schist	ND
K2	schist	FC, V
K3E	porphyry	F, B, V
K3W	schist	F, B, V
Topyurt	porphyry	V

864 *B: Brecciated, F: Fractured, FC: Foliation Changes, ND: Not Deformed, V: Veined

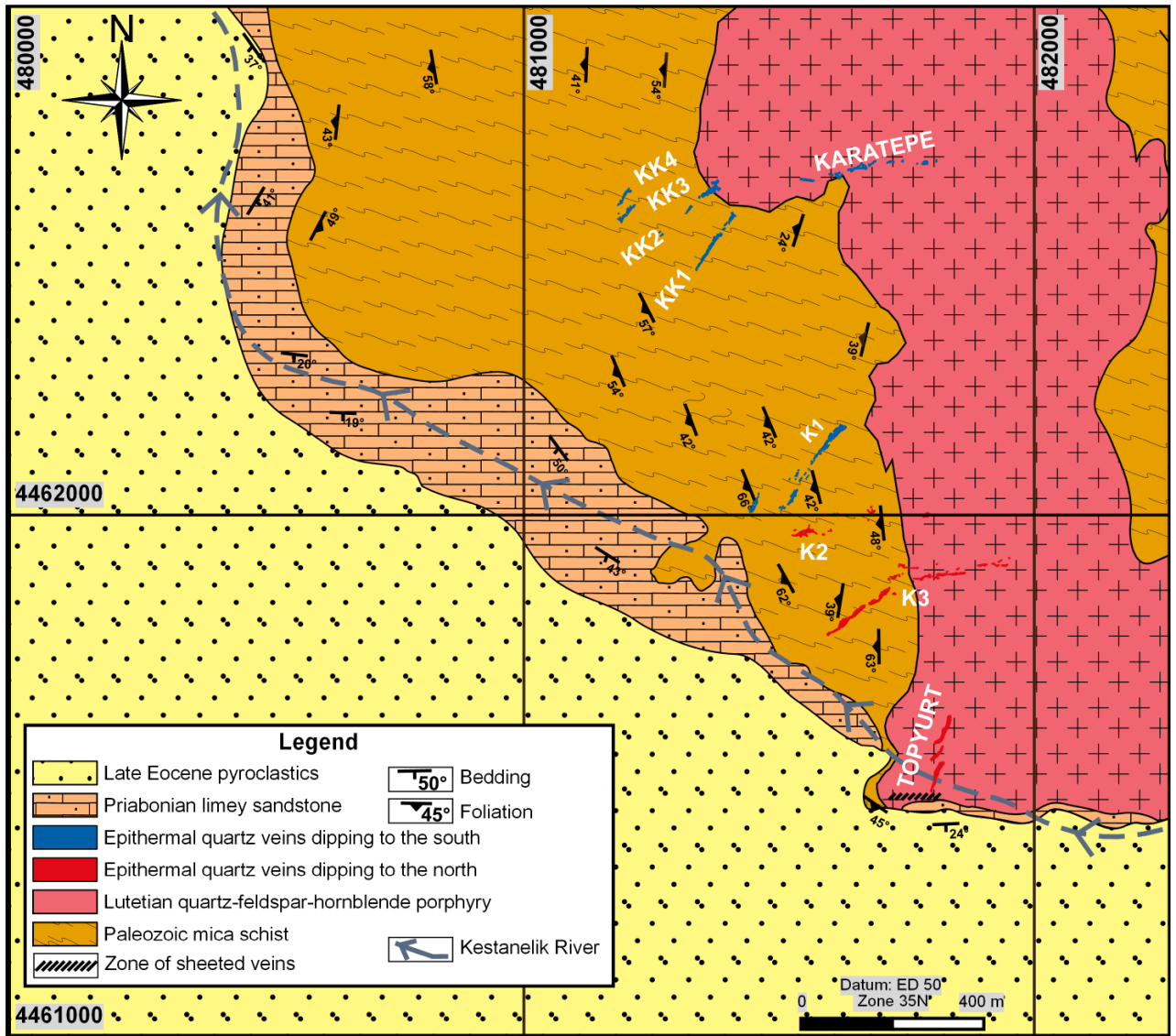
865

866 **FIGURES**



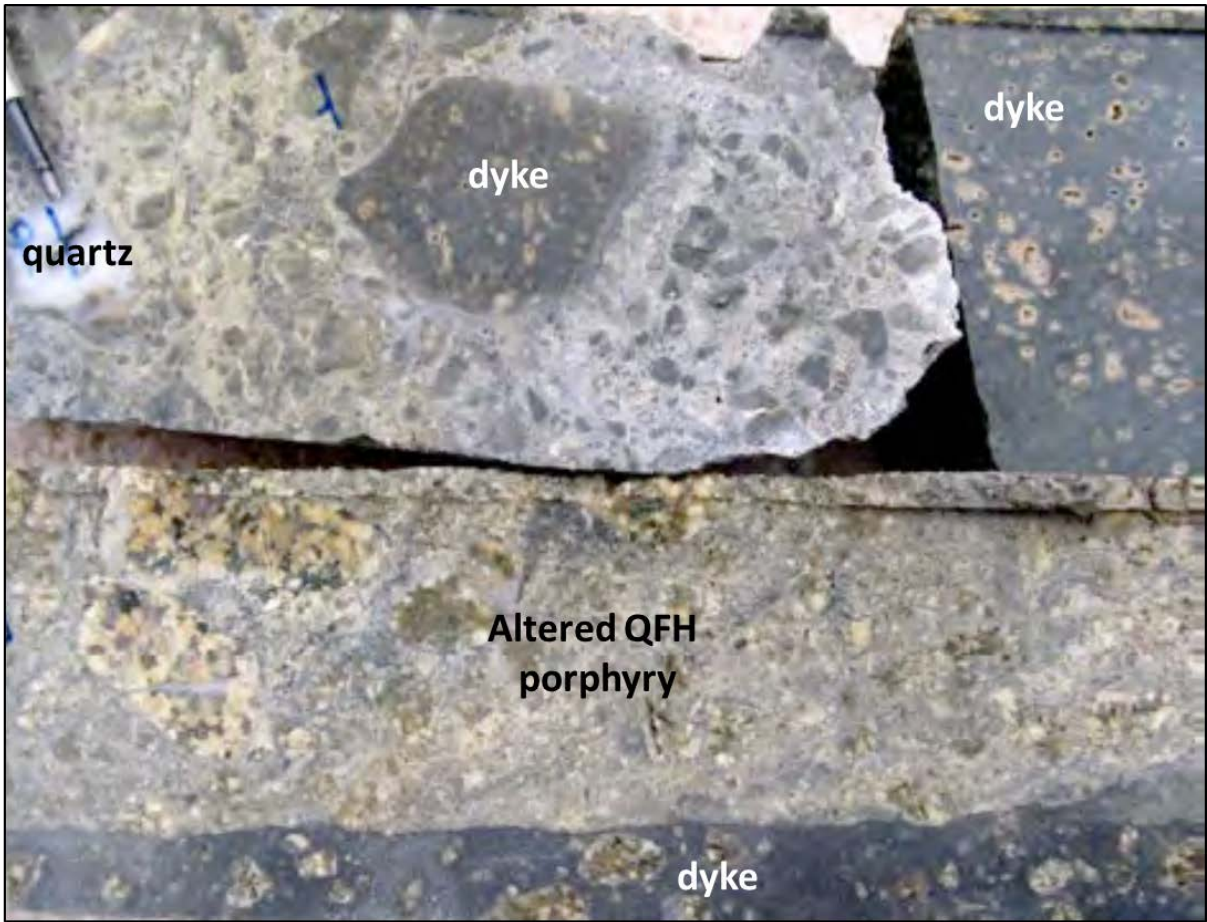
867

868 Figure 1



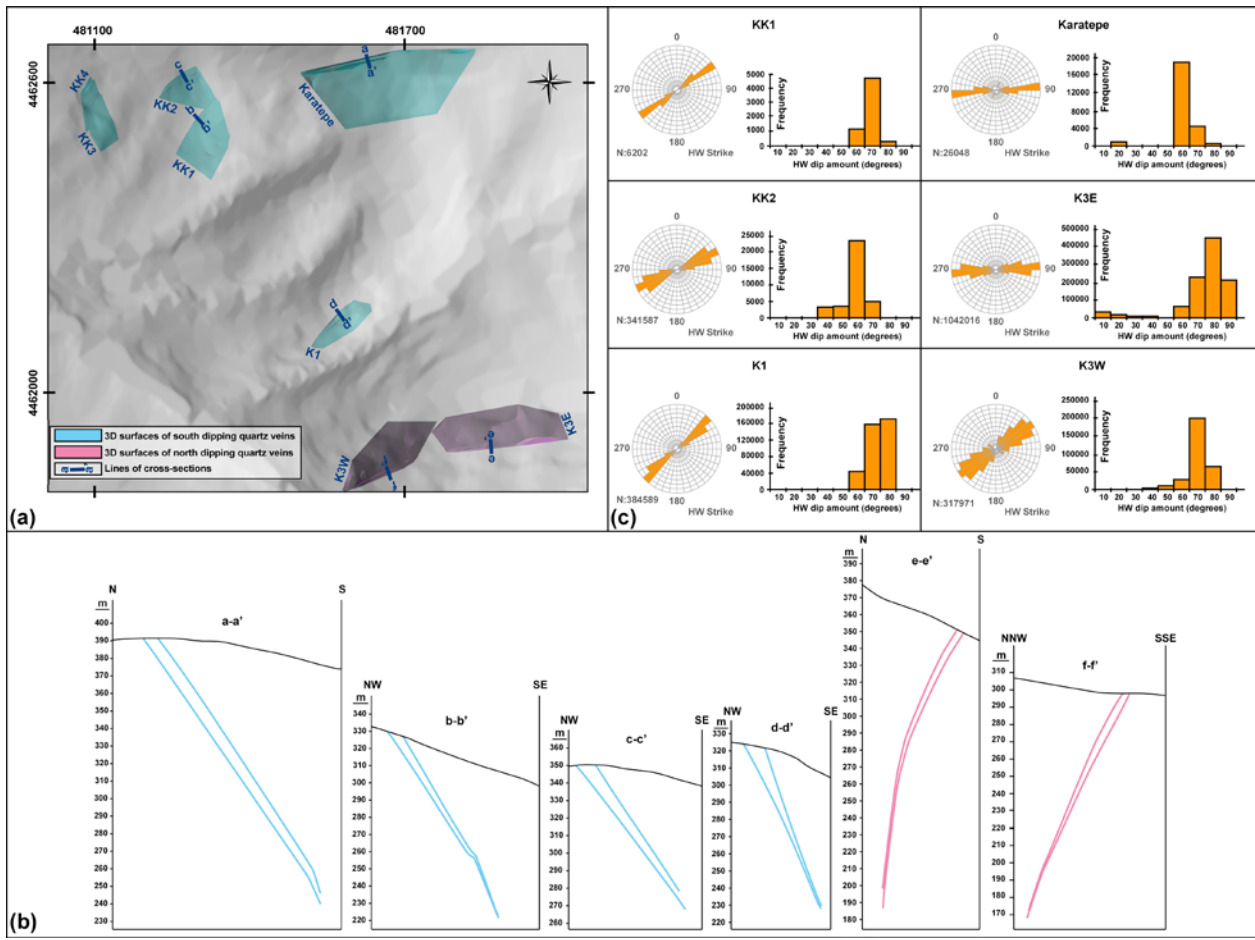
869

870 Figure 2



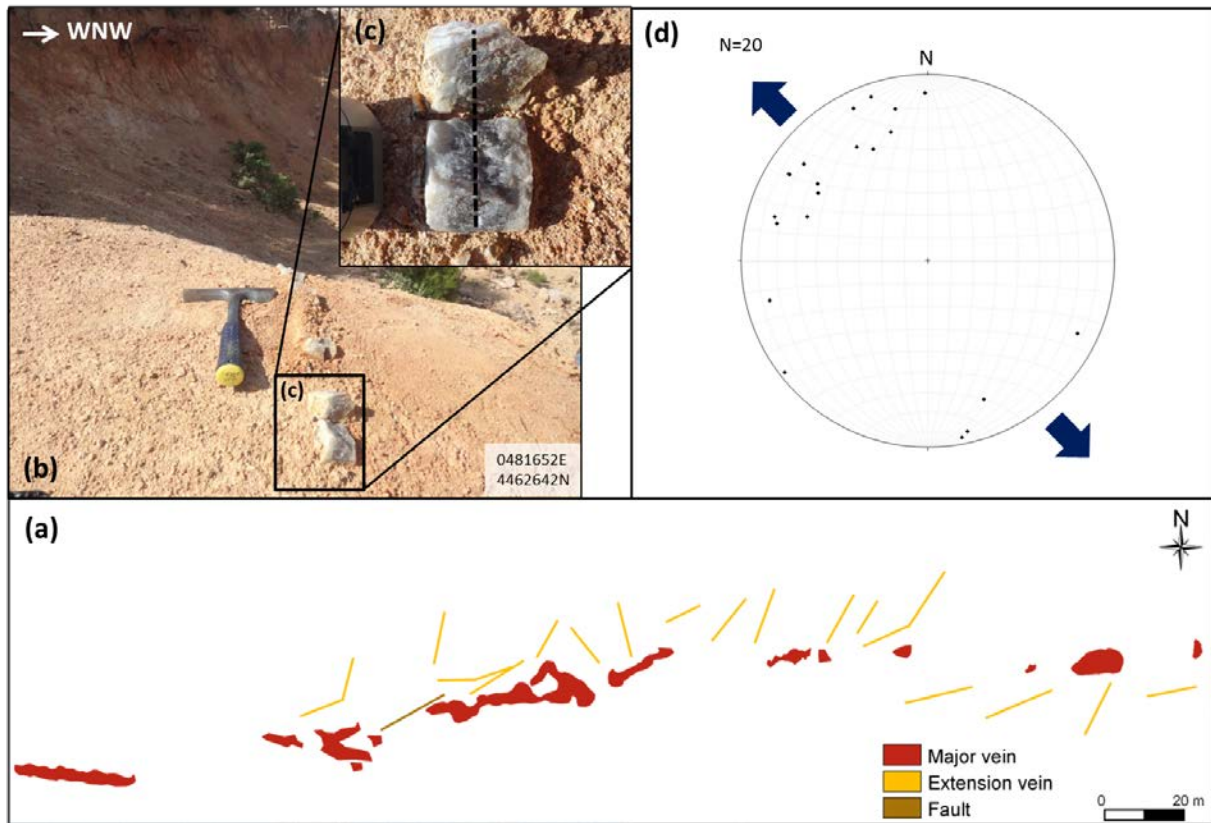
871

872 Figure 3



873

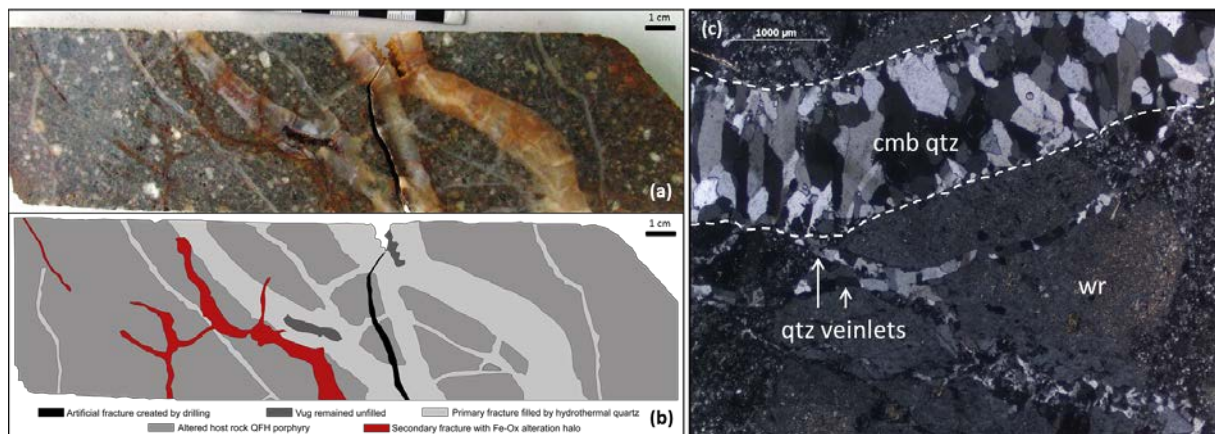
874 Figure 4



875

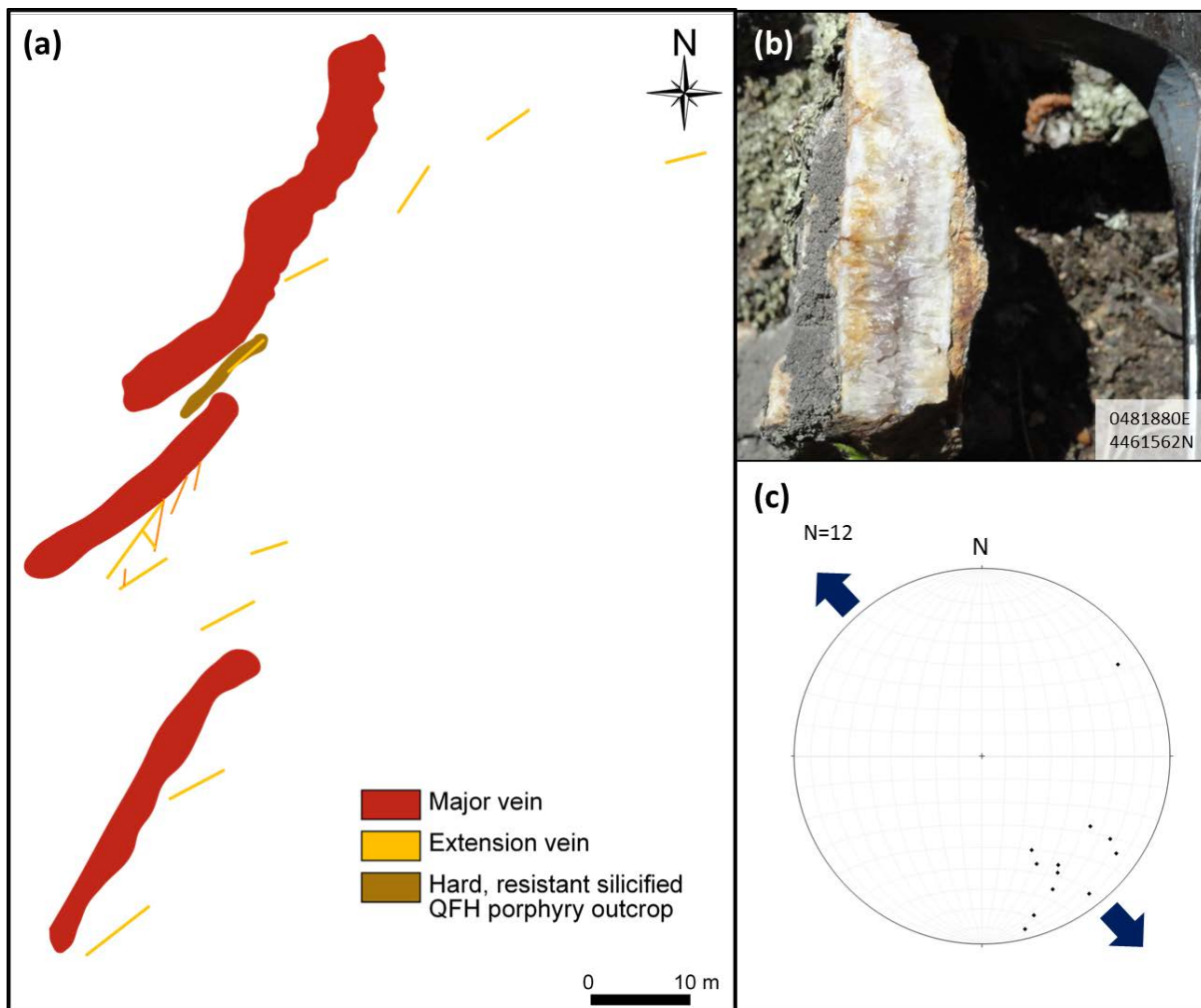
876 Figure 5

877



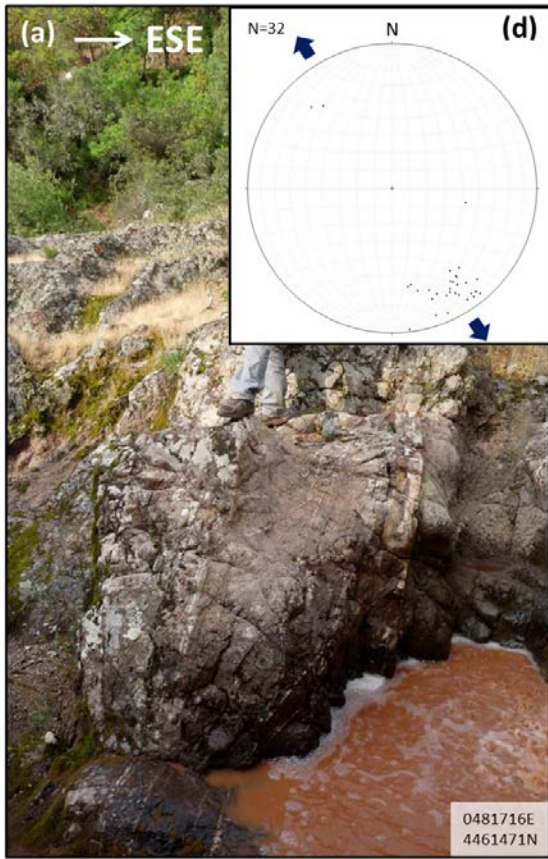
878

879 Figure 6



880

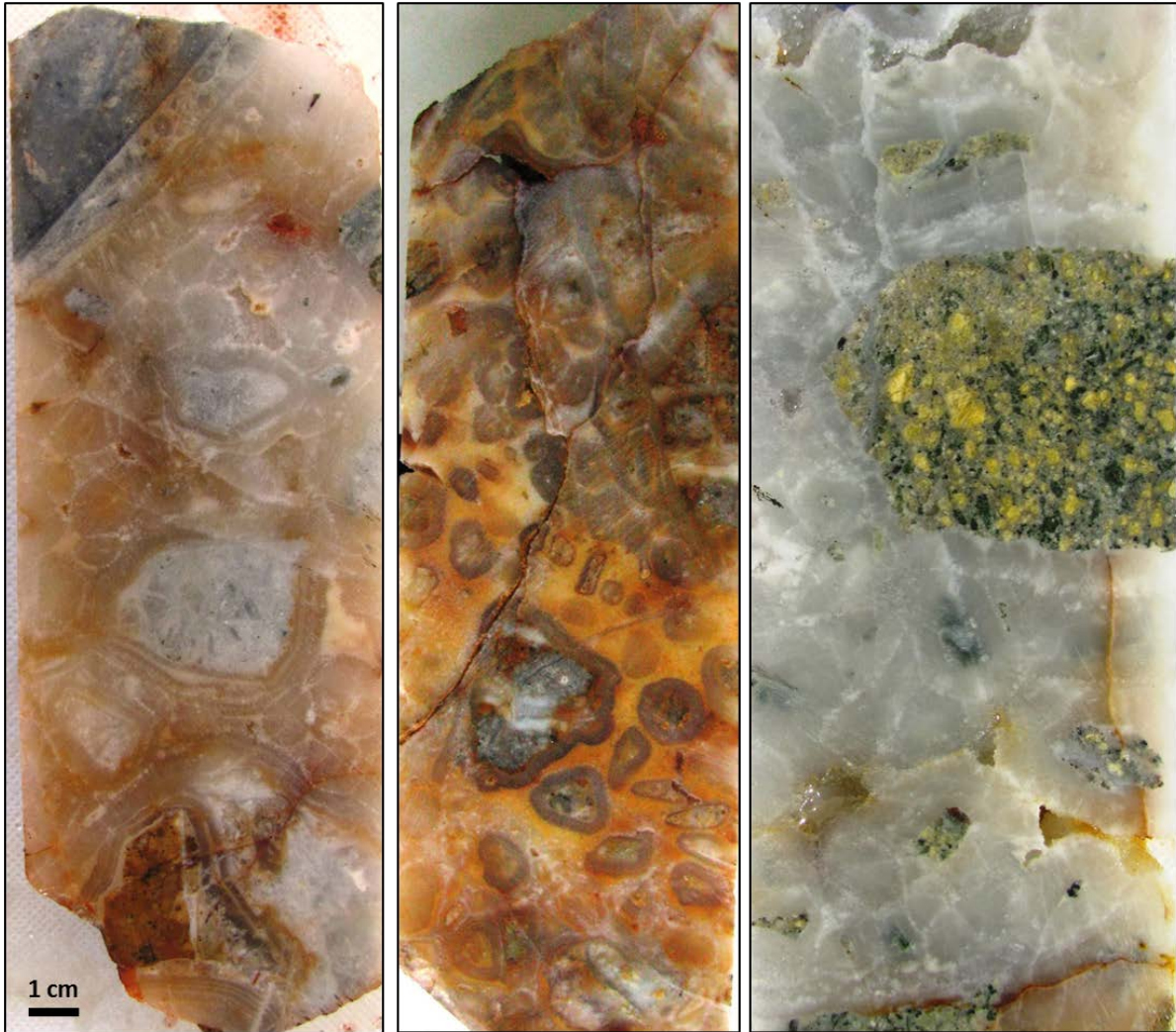
881 Figure 7



882

883 Figure 8

Elevation decreases (depth increases) →



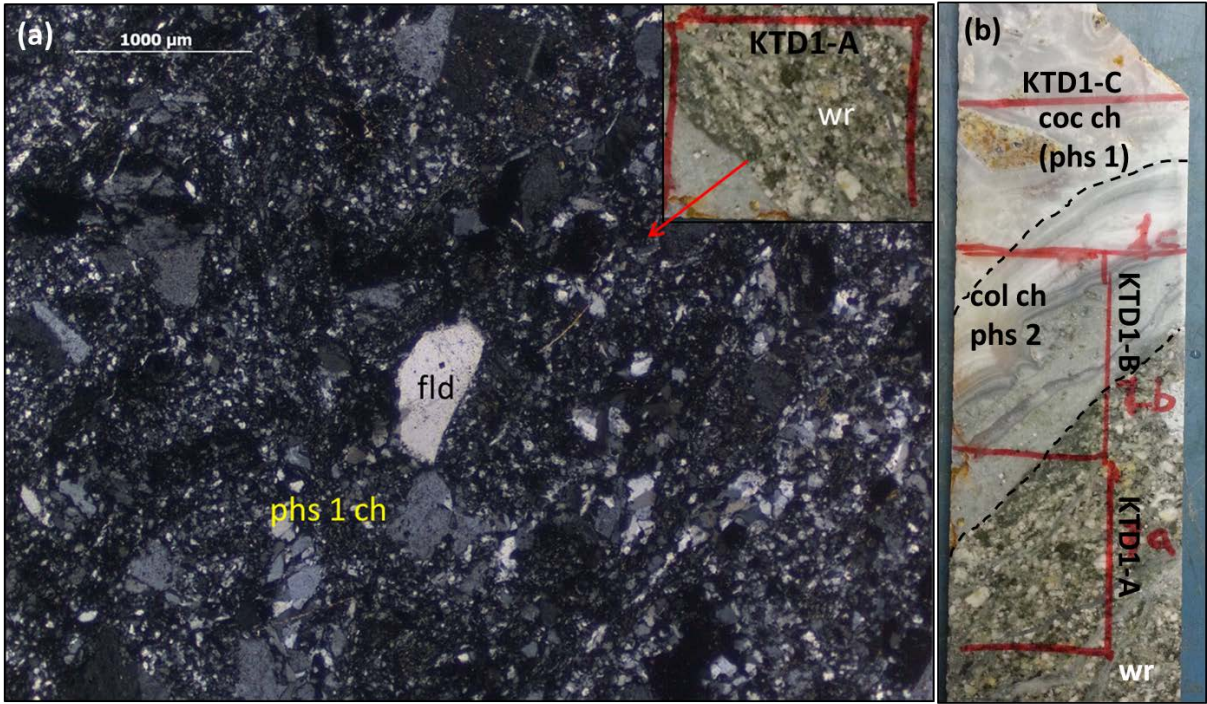
KED-43 14.9 m
(387.5 m asl)

KED-18 128.1 m
(264.4 m asl)

KED-16 123.6 m
(238.2 m asl)

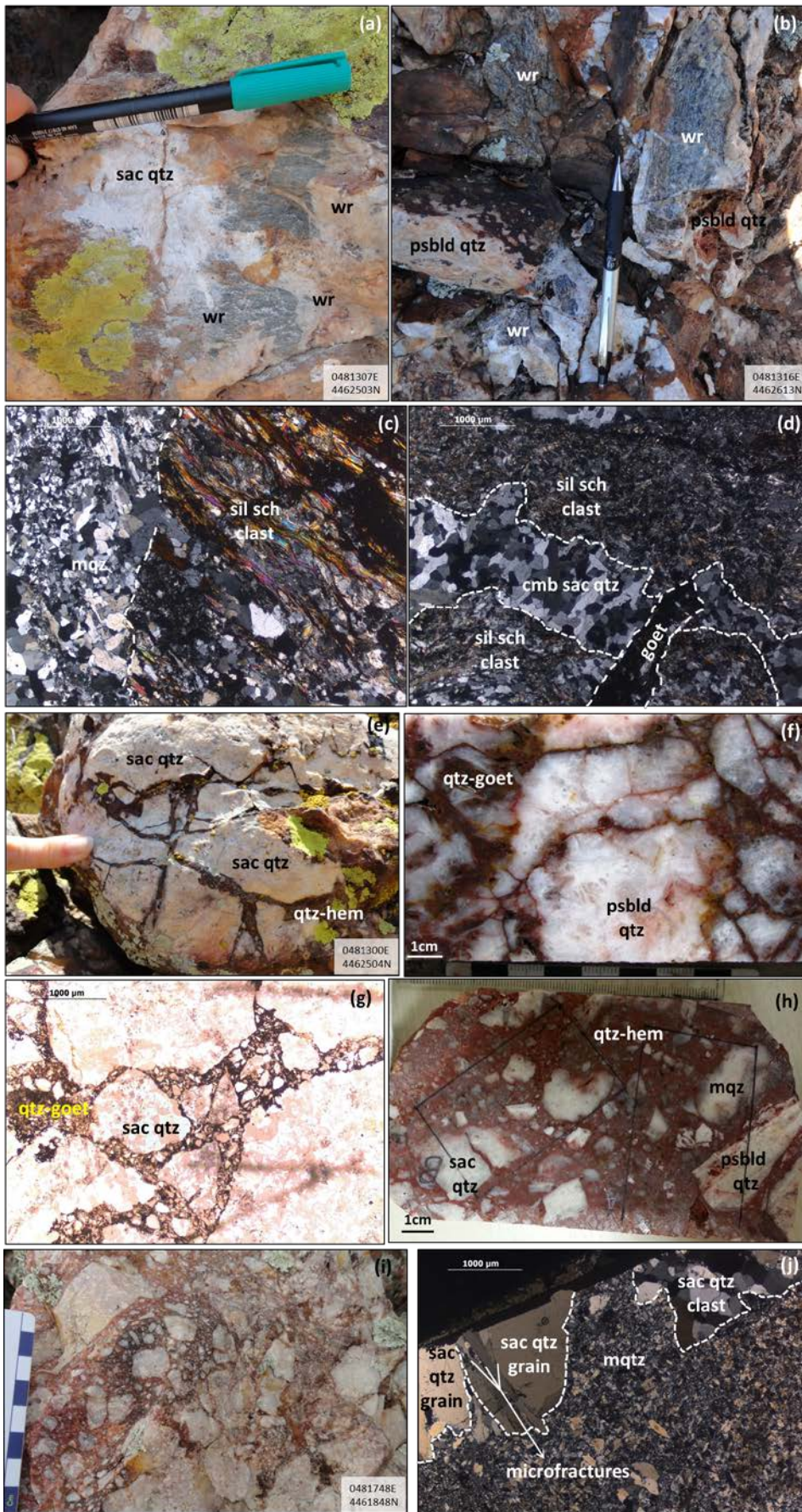
884

885 Figure 9



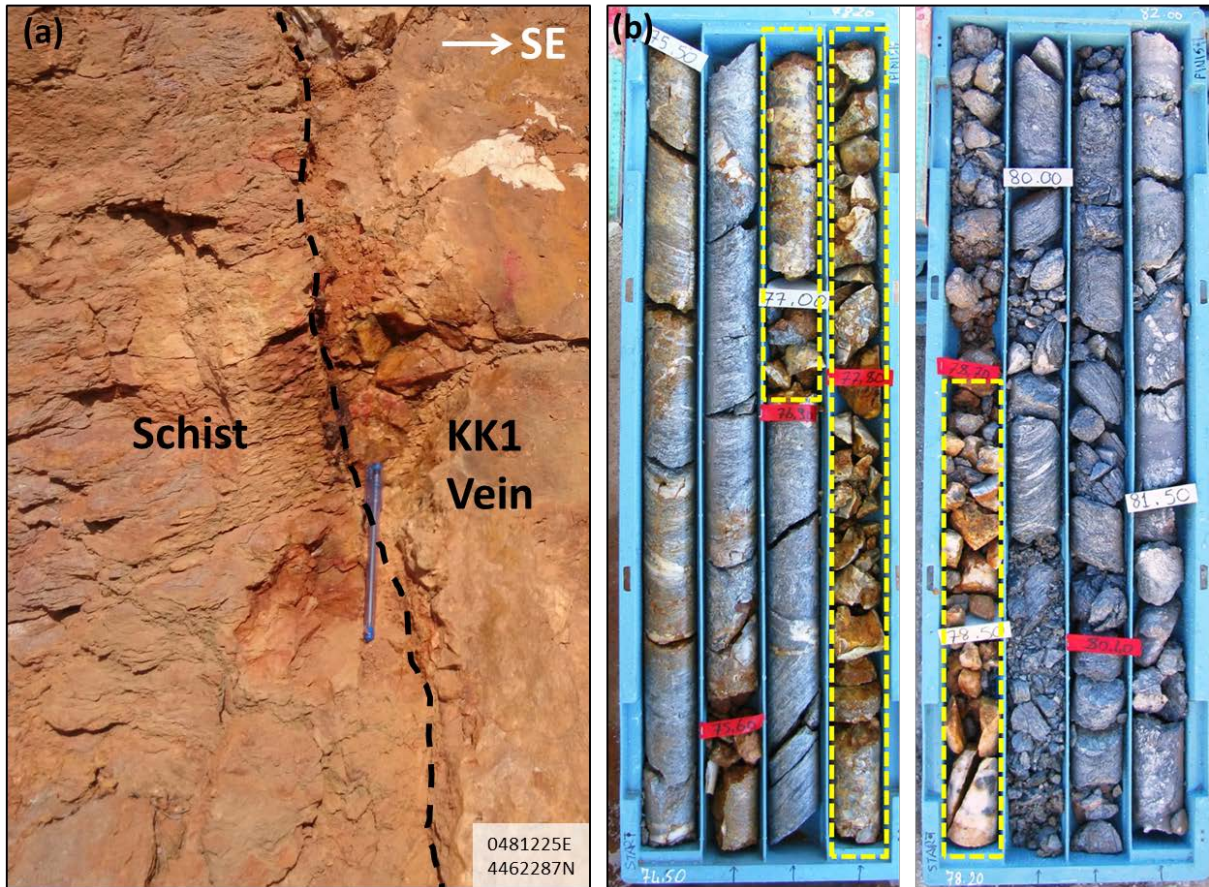
886

887 Figure 10



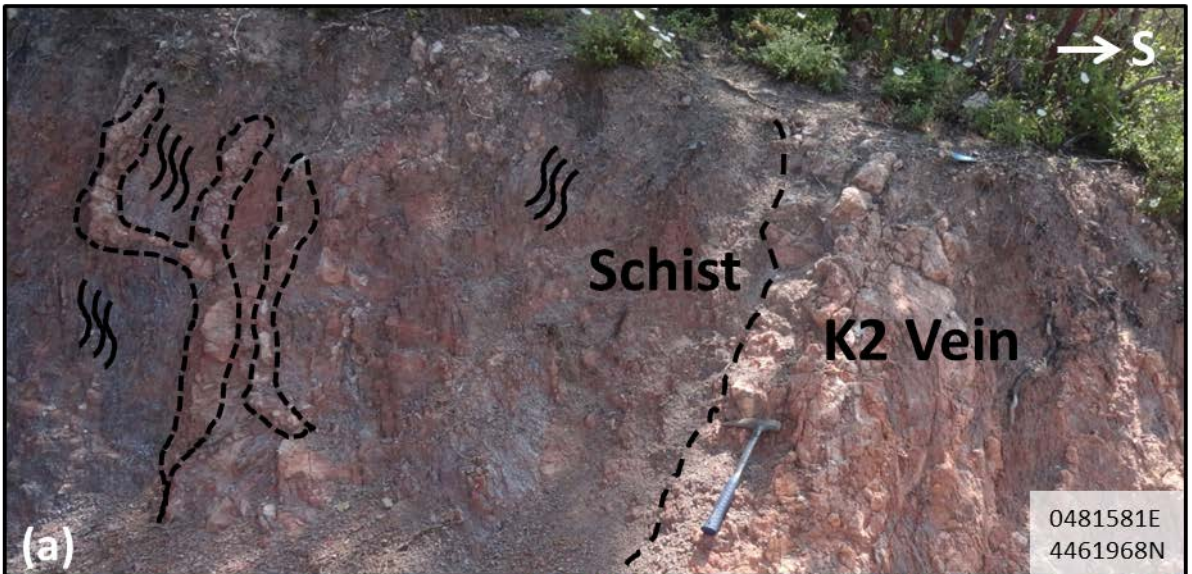
888

889 Figure 11



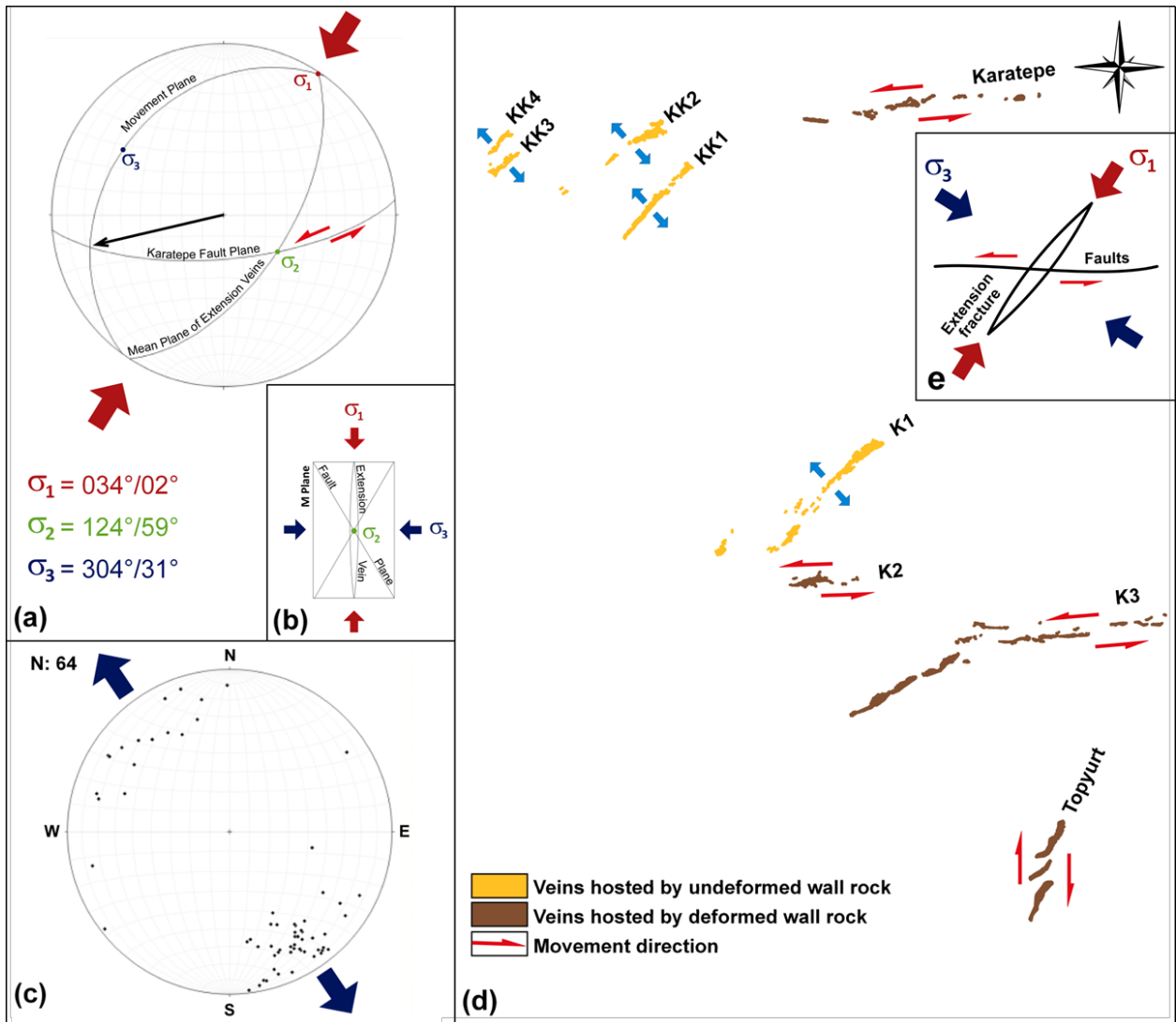
890

891 Figure 12



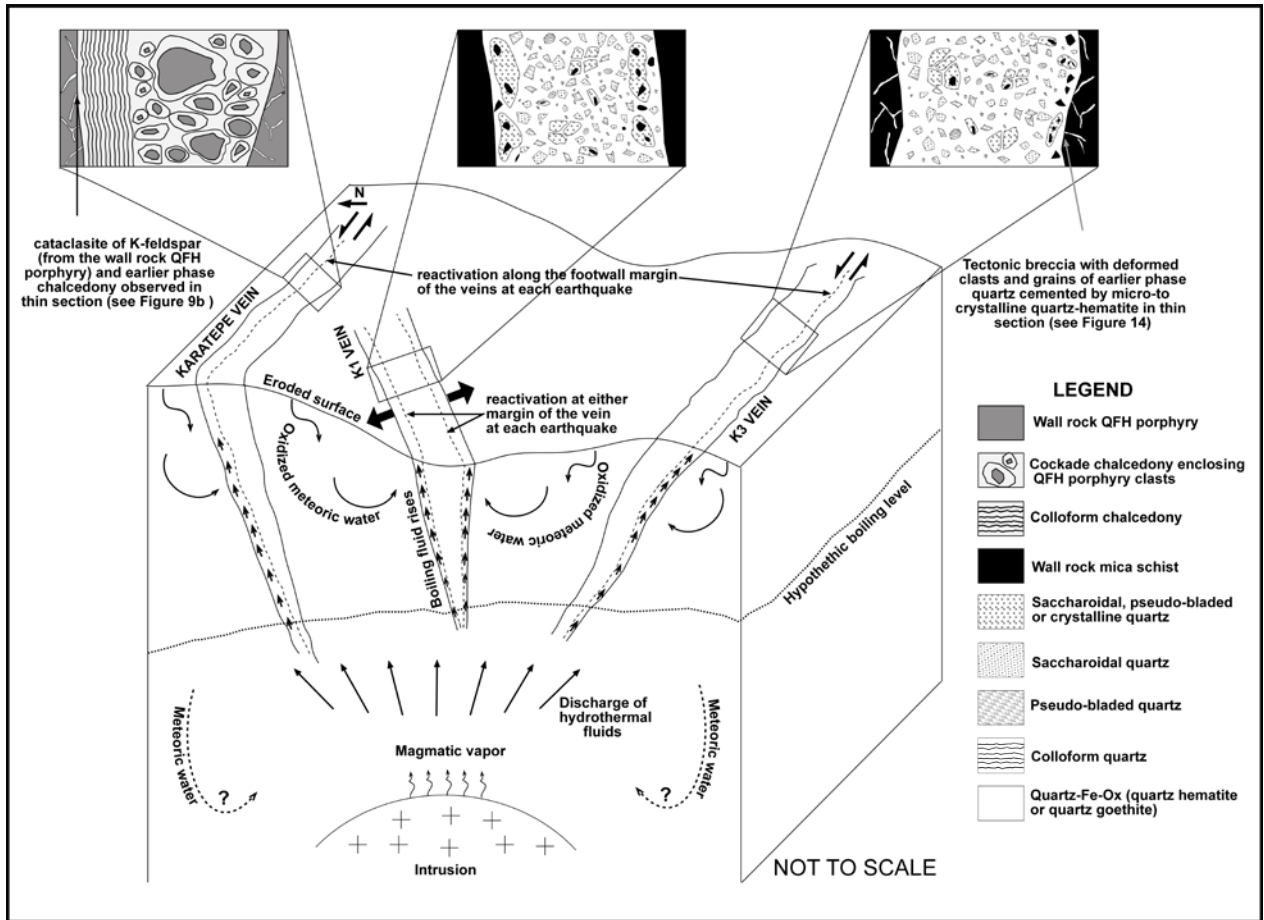
892

893 Figure 13



894

895 Figure 14



896

897 Figure 15